May 2016

# Analysis, Design and Implementation of a Resonant Solid State Transformer

Mohamad Zouheir Sabbah
*University of Wisconsin-Milwaukee*

# ANALYSIS, DESING AND IMPLEMENTATION OF A RESONANT SOLID STATE TRANSFORMER

by

Mohamad Sabbah

A Thesis Submitted in

Partial Fulfillment of the

Requirements for the Degree of

Master of Science

in Engineering

at

The University of Wisconsin-Milwaukee

May 2016

# ABSTRACT

## ANALYSIS, DESING AND IMPLEMENTATION OF A SERIES RESONANT SOLID STATE TRANSFORMER

by

Mohamad Sabbah

The University of Wisconsin-Milwaukee, 2016

Under the Supervision of Professor Adel Nasiri, PhD

This thesis discusses the design of a full-bridge resonant LLC Solid State Transformer. The proposed topology uses a high-frequency transformer which helps minimizing its cost and size, and enables operating at varying load conditions. By using a resonant circuit, soft switching is achieved. Commutation techniques are discussed, namely ZVS and ZCS. Both concepts are applied on different legs of the H-bridge. Pulse frequency modulation (PFM) and Phase Shifting Modulation (PSM) are utilized to control this resonant converter. One of the requirements of this work is to achieve a tightly regulated DC bus voltage. This was shown to be achieved using the proposed controller. An experimental setup was assembled and the controller was tested, the results match the simulation and calculation results. The SST setup was tested for two different power levels. The outputs confirm the validity of the controller in feeding the load and regulating the voltage within the desired switching frequency interval, while maintaining soft switching. A thermal analysis was conducted to calculate losses, and a conversion efficiency of 97.18% was achieved. Using a high frequency transformer, a reduction in size and cost is achieved as compared to conventional low frequency transformers that usually are large in size and require more material to be assembled (copper and iron). Design requirements and limitations, the

proposed control scheme, modeling and implementation, and test results are provided in this thesis.

*Dedicated to my parents for their infinite love and support.*

# TABLE OF CONTENTS

## LIST OF FIGURES

# LIST OF TABLES

## LIST OF ABBREVIATIONS

AC – Alternating Current

DC – Direct Current

CCM – Continuous Conduction Mode

DCM – Discontinuous Conduction Mode

EMI – Electromagnetic Interference

$F_s$ – Switching frequency

$F_r$ – Resonant frequency

IGBT – Insulated Gate Bipolar Transistor

PLR – Parallel Loaded Resonant

SiC- Silicon Carbide

SLR – Series Loaded Resonant

SST- Solid State Transformer

# ACKNOWLEDGMENTS

I would like to express my great gratitude to my advisor Dr. Adel Nasiri. His advice and guidance has been extremely helpful. During my masters I learned much about engineering and research, and I have learned much beyond that.

Many thanks to Dr. Rob Cuzner for his continuous help and advice during my research. His suggestions were highly important. I would like to thank Dr. Dan Ionel for his endless advice.

I gratefully acknowledge my colleagues and friends in the Power Electronics team at UWM. Working with you all has been of great pleasure.

Finally, my deepest gratitude goes to my family for their utmost love and support. I would like to thank my Uncle for his selfless and endless help.

# CHAPTER I

## 1. INTRODUCTUON

There is a shift in the years-old model of energy generation and distribution. The emerging concept integrates various elements including Distributed Generations (DG), energy storage, DC systems, and power electronics-based systems. Future electric distribution systems could be an interconnection of microgrids with various DC or AC voltage levels. A future distribution system is shown in figure 1-1. The conventional 60Hz transformers cannot meet the flexibility and controllability demanded by this new model. The subsystems are interconnected via power electronics based isolated converters, smart transformers or Solid State Transformer (SST).

Solid state transformers have been formulated by several researchers since the late 1990s [1-3]. In their essence, they combine power electronics converters and high- and medium-frequency transformers to connect two systems at various voltage levels and types (AC or DC). If active converters are used for both SST ends, bi-directional power flow can be realized. Since a medium- or high-frequency transformer is used to create galvanic isolation, the size and cost of the SST is generally much less than a 60Hz transformer.

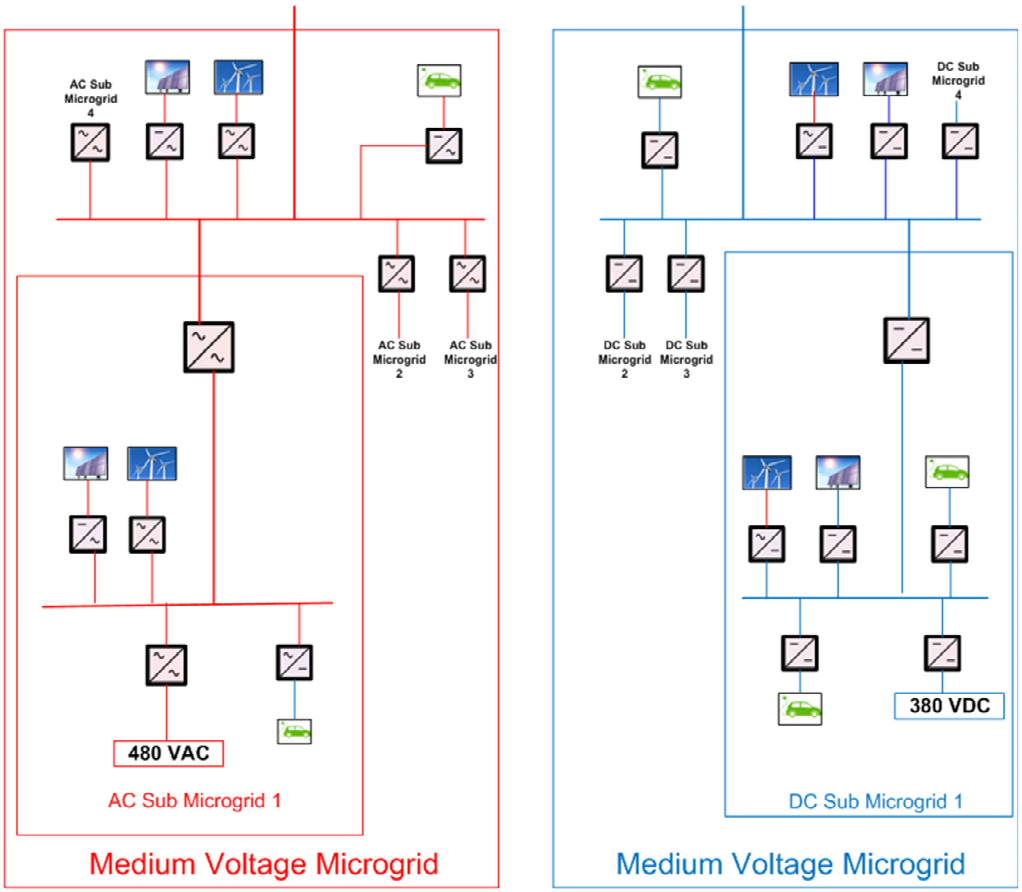


Figure 1-1: Zonal microgrid schematic.

SSTs can be used to offer several functionalities in a smart grid configuration including (i) protecting loads from power system disturbances, (ii) protecting the power system from load disturbances, (iii) integrating energy storage (energy buffer), (iv) providing DC ports for distributed generation connection, and (v) supporting voltage and power profiles. SSTs can play an important role in realizing the next-generation integrated power system (Figure 1-1). They will link the medium voltage microgrid to the transmission system as well as low voltage AC and low voltage DC systems.

Energy storage elements are an important element in modern distribution and generation. They can be integrated on the DC link of the SSTs to support the loads. SSTs

can also provide reactive power to support voltage stability at various voltage stages. Inclusion of voltage and current sensing and communication capabilities in SST configurations can enable load support, transient stability improvement, and fault isolation, which leads to higher reliability and survivability. One of the main concerns in realizing SST topologies is energy conversion loss in multiple high frequency conversion stages. Applying resonant behavior to these topologies can significantly improve the energy efficiency. A few researchers have recently published on techniques to add resonance to SST structures.

## 1.1 Literature review

In [4], the authors describe a CLLC topology for a bidirectional SST for DG interface. A complex dead-band control at sub resonant frequency is used and the switching frequency is limited at the resonant frequency. Although the proposed converter achieves a relatively high efficiency, limiting the operation below the resonant frequency has many disadvantages. First disadvantage is the inability to make use of the natural turn on at ZVS of all the switches in the h-bridge. Switching at super resonance, however, ensures soft commutation at turn on. Another disadvantage is sizing the components of the converter and the filter. In this paper, the switching frequency is in the order of 50 kHz, where the resonant frequency is 65 kHz. That means that the resonant frequency is pushed to 65 kHz by sizing the components of the resonant tank to ensure switching is in DCM mode (below resonance).

In [5], the authors describe a three-level resonant single-stage PFC converter suitable for high power applications. Variable frequency phase shifted modulation (VFPSM) is used,

and switching frequency is limited above resonant frequency to achieve ZVS, whereas ZCS operation is not analyzed. In this paper, a three level resonant converter is discussed. The first level is controlled by phase shifting and provides a boost function. The final level is frequency controlled and regulates the output voltage across the load. Due to limitations on the duty ratio discussed in the paper, the converter can only operate in DCM mode. Additionally, the achieved efficiency was 91.5%.

The authors in [6] discuss a design methodology of bidirectional LLC resonant SST. A dual half bridge (DHB) is used in the middle stage in the targeted single phase topology. Analysis and experimentation limits the switching frequency around the resonant frequency. Soft commutation was achieved, namely ZVS for the active switches, and ZCS for synchronous rectifiers. The paper, however, doesn't describe the used control structure.

In [7], the authors discuss a frequency tracking control for a bidirectional resonant DC/DC converter (DAB converter). The resonant converter is coupled with a buck/boost stage converter. Figure 1-2 shows the proposed topology. The authors propose a frequency tracking control method to regulate the output voltage. The controller works as explained in figure 1-3. In a fixed frequency control method, the controller as to adjust the gain (to regulate) by going from point A to point C. In a conventional frequency control method, the controller adjusts the gain by going from point A to B. By using a frequency tracking control method, the controller goes from point A to D. This would be accomplished by using PWM on the buck/boost converter to adjust the duty cycle, where frequency control is realized by adjusting the switching frequency on the H-bridge.

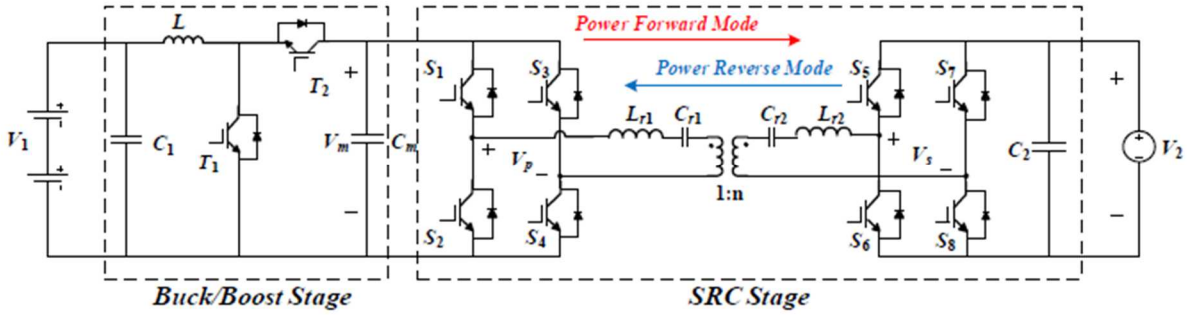


Figure 1-2: Buck boost converter coupled with a high frequency DAB converter.

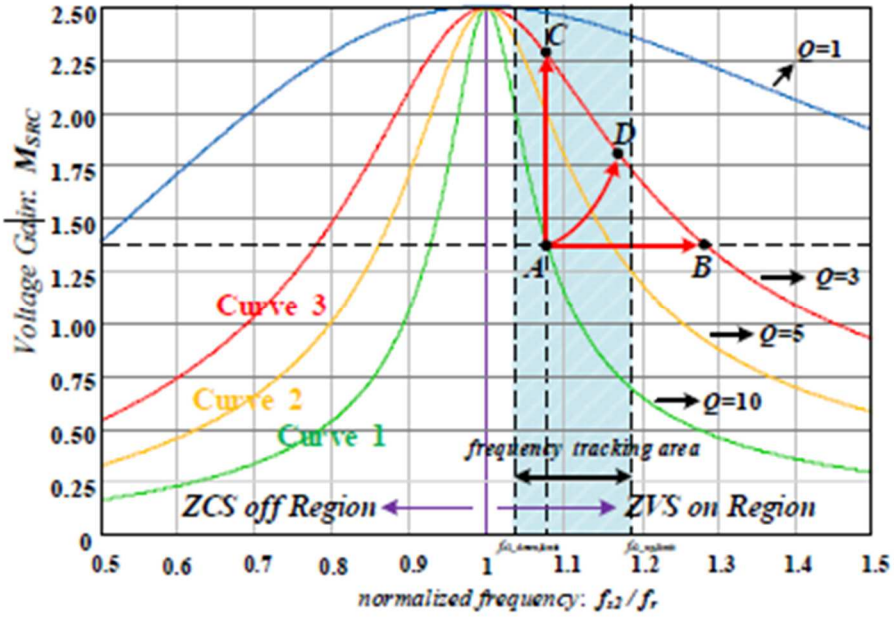


Figure 1-3: Frequency tracking control concept.

The switching frequency is limited below the resonant frequency. One of the disadvantages observed in this work is turning off at finite current. This causes losses and stresses across the switches. The peak efficiency achieved in this paper is 96.5%.

Additionally, Zero crossing detection is used to achieve soft commutation. The drawback of using a detection circuit is that it causes a phase lag.

In [8], a detailed theoretical analysis and design of an LLC resonant converter is presented. The transfer function of output voltage to input voltage is derived and is used to plot the gain curve of the resonant converter. Three regions are identified in the gain curve plot as shown in figure 1-4. Additionally, design limitations on the sizing of many parameters of the system are analyzed and presented. The design requirements of the magnetizing inductance $L_m$, dead time, switching and resonant frequency, and resonant capacitor are discussed. Experimental results for a 400W prototype are provided in this work. The control method, however, is not discussed.

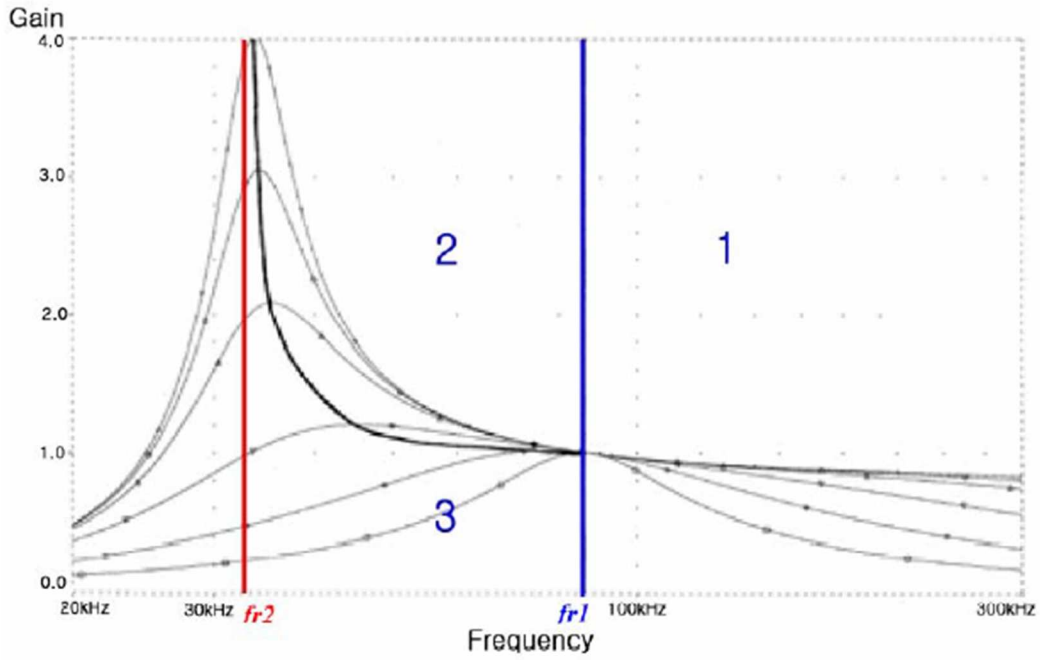


Figure 1-4: Gain of resonant converter plotted versus the switching frequency.

In [9], an interleaved LLC resonant converter topology is presented. Two converters are connected in parallel to support one load. Pulse frequency modulation (PFM) is used to regulate the voltage on the output, where phase-shift modulation (PSM) is used to adjust the mismatch of current output of the two converters. ZVS and ZCS conditions are analyzed. It is concluded in this paper that operating below the resonant frequency is suitable for this application and for wide input and output voltage variations. Efficiencies achieved in this paper are in the range from 78% to 82% depending on the load, operating frequency, and duty ratio. Duty ratio is decreased when PSM method is applied. Operation in this paper, i.e. switching frequency, is limited below the resonant frequency.

In [10], the work is focused on the detailed mathematical modeling of a resonant full-bridge converter. Generalized state space averaging method is used for linearization, and matrices A, B and C are obtained. Simulation results are provided, where a simple PSM controller is used to regulate the voltage. Operation is limited at a fixed switching frequency. The resonant frequency is 50.6 kHz and operation is slightly above resonance at a switching frequency of 55 kHz.

In [11], an LLC resonant converter is presented for induction heating applications. A full bridge inverter used, and power is regulated by adjusting the phase shift only on switch four of the topology. This results in cancelling part of the positive half cycle where the duty ratios corresponding to the negative half cycle are not changed throughout the operation. Therefore, an asymmetrical square wave voltage is seen at the terminals of the h-bridge. This causes heating which is required for such applications. Also, the switching

frequency is slightly adjusted by using a phase-locked loop for sensing zero crossings. The switching frequency is limited above the resonant frequency, and it's varied between 108.8 kHz and 110.6 kHz.

In [12], the same authors discuss the asymmetrical voltage cancellation method presented in [11]. In this paper, the controller is capable of changing the switching frequency as well as the phase shift on switch 4 in the h-bridge inverter. This results in better dynamics to support larger load range and input voltage variation. The proposed control structure is called variable-frequency asymmetrical voltage cancellation (VFAVC). Switching frequency is limited above the resonant frequency to ensure ZVS operation of the switches. Better ZVS range and hence a better efficiency is achieved implementing a variable-frequency control.

In [13], a variable frequency phase shift modulation technique for a dual active bridge is presented. The topology allows for bidirectional power flow by using active switches on both side of the transformer. A detailed analysis for power transfer using phase shifting between the primary and secondary h-bridges is presented. In addition, conditions for meeting ZVS operating by ensuring enough dead time before switching are discussed, where different scenarios are shown. The proposed operation method ensures either ZVS or ZCS on a wide load range. Depending on parameters selection and controller operation, either ZVS or ZCS is employed depending on the value of current at which the switching is done. The duty ratios of the switches are not altered which limits the supported power range of the converter as well as its ZVS operation.

In [14-17], different authors talk about multiport SST's and converters. In [14], d-q vector-based common-duty-ratio controller for a single-phase multilevel active rectifier is presented. In addition, the same concept is applied for output-paralleled DAB converters. For the cascaded rectifier, switching frequency of 10 kHz is used. For the DAB module, the switching frequency is 20 kHz. For the experimental part, a 3-KVA SST prototype is tested. The testing results show the capability of bidirectional power flow, and the used switching frequency is 5 kHz. This low switching frequency is the reason why it takes 8 complete cycles to finish the process of transferring the renewable energy to the grid.

In [15], a multiport DC-DC SST is discussed. This work also discusses soft commutation (ZVS) in such multiport topologies. Multiple modular converters were taken into account in the course of this study. Two control approaches were followed to design the controls for the SST DC-DC stage: SISO and MIMO. SISO stands for single-input-single-output and MIMO stands for multiple-input-multiple-output. Testing was performed on a 1KW unit with a switching frequency of 20 kHz.

In [16], a quad-active bridge (QAB) is analyzed. A single-input-single-output (SISO) approach for the controller is adopted for the multiple-port converter, and the AC-DC single rectifier is controlled using PWM. The proposed system incorporates the grid, PV array, energy storage and a load. All values of the topology's inductance, capacitances and voltages are given. The switching frequency is selected to be 20 kHz. A generic model for the multi-active bridge (MAB) is developed to design the controller.

The author [17] discuss dual-active bridge (DAB) and triple-active bridge (TAB) topologies. The design procedure of the proposed (TAB) is then discussed where various

parameters of the system are selected including inductances. The system is modelled to obtain a transfer function and controlled to regulate voltage and power flow based on current. The switching frequency is selected to be 5 kHz.

## 1.2 Thesis objective and layout

The objective of this thesis is to design and implement a resonant SST suitable for power distribution applications. The designed converter must be able to adapt to changes in the load and regulate the output voltage accordingly. The input voltage, output voltage and preliminary load requirements are summarized in the table below:

| Parameter | Rating | Unit |
|---|---|---|
| $V_{in}$ | 700 | VDC |
| $V_{out}$ | 1000 | VDC |
| High/Peak load | 10,000 | W |
| Low load | 470 | W |

Table 1: System specifications.

One other motivation behind this work is to reduce losses and stresses across the switching devices. A big concern that comes with SST's is the energy conversion loss. The more levels/stages an SST uses, the higher the losses. Additionally, switching at high frequency causes ringing, high dv/dt and high di/dt across the switches. This contributes to parasitic inductances and capacitances seen across the switches [18]. Therefore, switching at zero current and/or zero voltage is crucial in order to be able to operate at

high switching frequencies. Eventually, by switching at high frequency, components in the resonant tank and filter can be sized to be smaller. Therefore, a reduction in size is observed.

This thesis report is organized according to chapters as follows:

-Chapter 2 highlights relevant and important background information related to the contribution done in this work.

-Chapter 3 convers the mathematical analysis and design constraints for the proposed SST topology. The equivalent circuit is derived and the operating modes and principles are discussed in details. Additionally, resonance is explained in terms of the used topology.

-Chapter 4 discusses the used control structure, its parameters and implementation. Simulation results and disturbance response are discussed in this chapter.

-Chapter 5 shows the thermal analysis conducted to calculate losses and efficiency. The chapter goes over the software used to conduct the analysis and the associated results.

-Chapter 6 discusses the experimental testing performed on a prototype of the proposed converter.

-Chapter 7 summarizes the thesis accomplishments and provides insights for future work.

# CHAPTER II

## 2. BACKGROUND

When discussing power converters, two groups are considered: Linear and switch mode power supplies (SMPS). SMPS converters have been in the market for a long time and they are superior to linear power supplies. They exhibit several advantages like reduced size, reduced cost and higher efficiency. They do, however, require more complex control schemes and EMI filters.

SMPS topologies can be either isolated or transformer-less. An isolated topology includes a conventional transformer that operates at high frequency in some cases. Including a transformer adds several advantages, a few of which are:

- Operating the output voltage at higher or lower than the input voltage.
- Leveraging multiple windings transformers for applications of multiple outputs.
- Using the transformer windings as energy storage element instead of inserting an inductor.
- Providing electrical isolation by means of separating the primary and secondary stages by the windings of the transformer.

## 2.1 Transformer-less Converter Topologies

### 2.1.1 Buck Converter (step-down)

This is a basic transform-less converter topology that steps down an input voltage $V_d$ to an output voltage $V_o$, and hence the name buck converter. A few other more complicated topologies are based off this topology in terms of analysis and design. Figure

2-1 shows the circuit diagram of a buck converter along with a frequency spectrum of the output voltage.

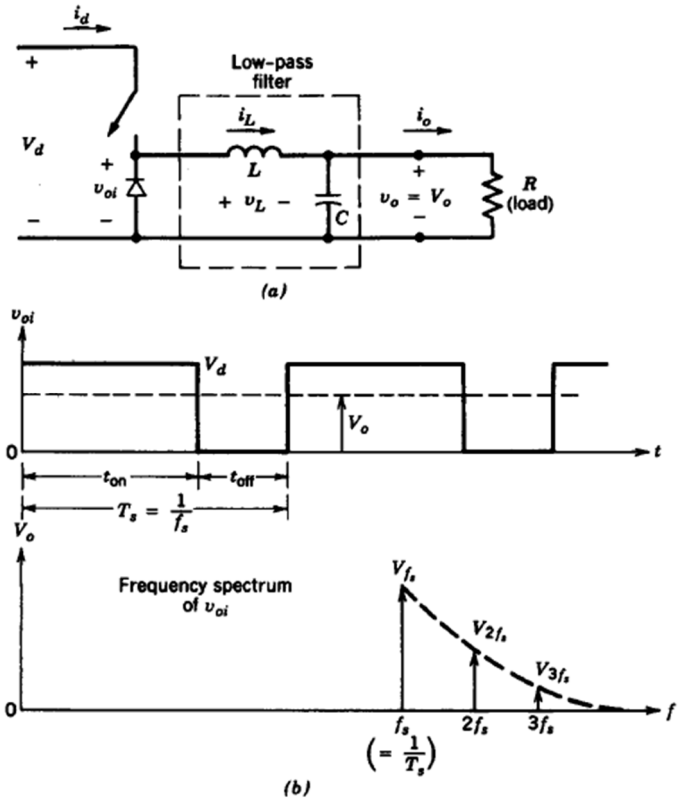


Figure 2-1: a) Buck converter b) Frequency spectrum of the output voltage [19].

This converters topology is the simplest and easiest to control. It has many advantages one of which is high efficiency. It is also suitable for high power applications, but EMI issues should be resolved with careful sizing of filters. Buck converters are regulated by adjusting the duty ratio of the switch. The inductor, which is the only energy storage element in the topology, changes when the switch is ON and discharges when it's OFF. Altering the duty ratio affects this charging and discharging cycle, resulting in a different average inductor current. The output stage is in series with the inductor, so change is directly seen on the output load.

### 2.1.2 Boost Converter (step-up)

This converter acts in an opposite way compared to the buck converter. The output voltage $V_o$ is larger than the input voltage $V_d$, the circuit diagram is shown in figure 2-2. This topology is suitable for power factor correction application due to its continuous conduction mode current.

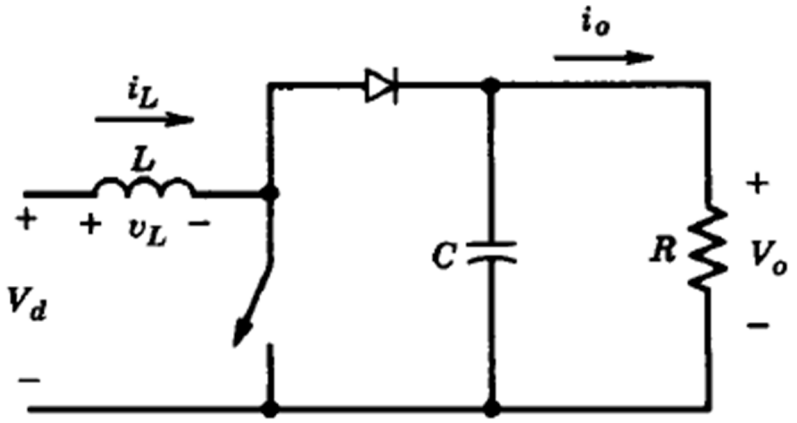


Figure 2-2: Boost converter [19].

Boost converters also have the advantage of being simple and easy to control. By adjusting the duty ratio, the output voltage is regulated. The duty ratio is generally limited before the parasitic effects become significant [19].

### 2.1.3 Buck-Boost Converter (step-down/step up)

A buck-boost converter combines the concept of operation of a buck converter and a boost converter, the circuit topology is shown in figure 2-3. The output voltage can be higher or lower than the input voltage. This allows for bidirectional power flow since the voltage can be either made to appear higher or lower looking from the output. Therefore, such a

topology suits energy storage applications (batteries) where power needs to be drawn or put in the battery at different times.

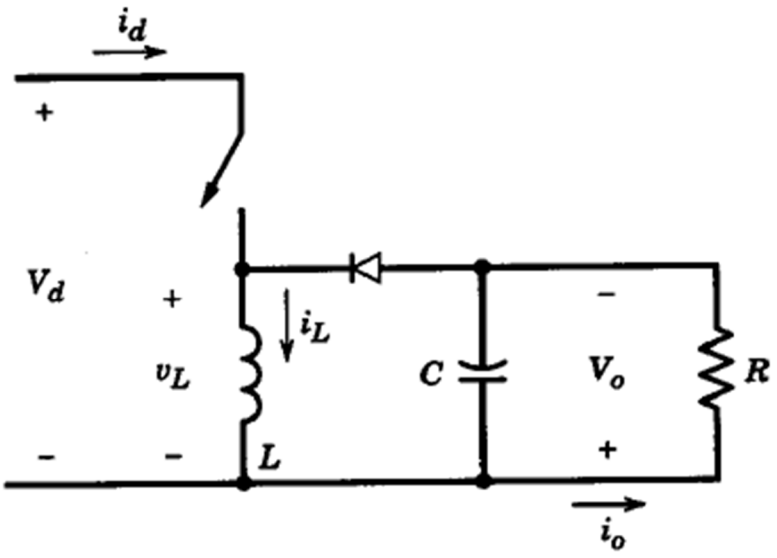


Figure 2- 3: Buck-boost converter [19].

Similar to buck and boost converters, buck-boost converters use only one inductor in their topology. Therefore, EMI analysis and inductor sizing is carried out in a similar manner. As in boost converters, parasitic elements have significant impact on the voltage conversion ratio and the stability of the feedback regulated buck-boost converter [19]. There is also an output voltage ripple that is reduced by carefully sizing the output capacitor.

### 2.1.4 Cuk Converter

Similar to buck-boost converters, Cuk converters can either step up or step down the input voltage. Cuk converters are considered to be the dual of buck-boost converters since a

capacitor is used as main energy storage and transferring element that transfers power between from the primary to the secondary stage.

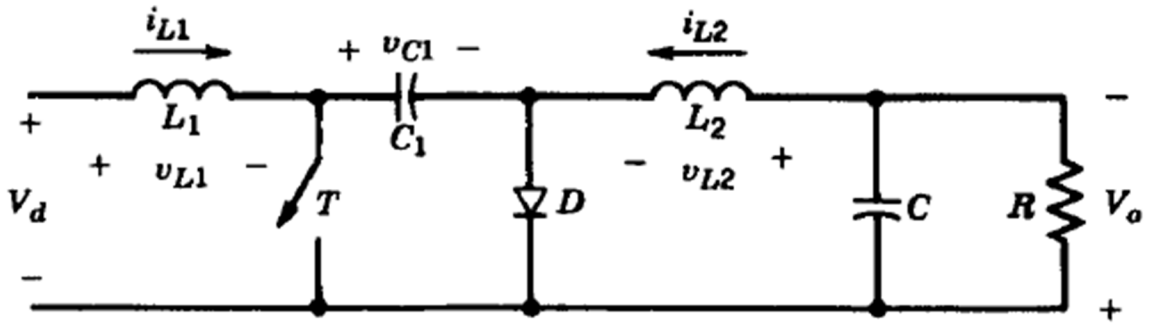


Figure 2-4: Cuk converter [19].

The assumption of a constant $v_{c1}$ in figure 2-4 is reasonable. One advantage of this topology is that both the input current and the current feeding the output stage are reasonably ripple free (unlike the buck-boost case where both currents are highly discontinuous) [19].

### 2.1.5 Full Bridge Converter

Full bridge converters are a very common topology. They have three main distinct applications [19]:

- Dc motor drives.
- Dc-to-ac (sine-wave) conversion in single-phase ac UPS systems.
- Dc-to-ac (high intermediate frequency) conversion in switch-mode transformer-isolated dc power supplies.

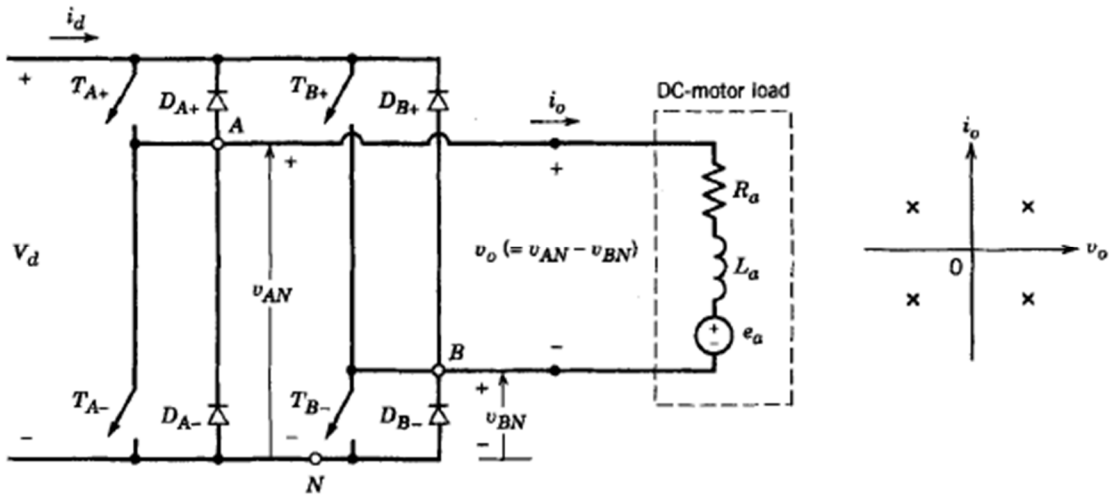


Figure 2-5: Full bridge converter [19].

In those three applications, the full-bridge topology doesn't change. In figure 2-5, the input is a fixed DC voltage and there is a DC load on the load. A full-bridge converter can operate in all four quadrants of $i_o$ and $v_o$ (output current and voltage) and permit bidirectional power flow. The type control, however, depends on the application. For the application described in figure 2-5, two common control schemes are used:

- PWM with bipolar voltage switching.
- PWM with unipolar voltage switching.

## 2.2 Isolated Converter Topologies

Isolated topologies include a conventional transformer. This transformer provides electrical isolation and helps in protecting against or minimizing the effect of faults. Isolated topologies can be grouped in two groups depending on the means by which electrical isolation is provided:

- Unidirectional core excitation.

- Bidirectional core excitation.

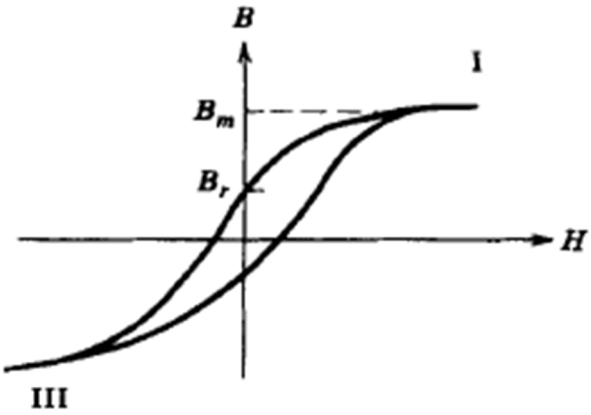


Figure 2-6: Typical B-H loop [19].

Unidirectional core excitation means that only the positive quadrant (quadrant I) in figure 2-6 is used. Bidirectional core excitation corresponds to using both the positive and negative quadrants (I and III) in the B-H loop.

Some of the dc-dc converters that are without isolation can be modified to provide electrical isolation by means of unidirectional core excitation. Two examples are:

1) Flyback converters (derived from buck-boost converters).
2) Forward converters (derived from step-down converters).

PWM switching is used to regulate the output of these converters. To provide bidirectional core isolation, the following topologies can be used to produce a square-wave ac at the input of the high-frequency isolation transformer:

1) Push-pull.
2) Half bridge.
3) Full bridge.

The above isolated three topologies are controlled by PWM scheme, which controls the interval 'Δ' during which all the switches are off. This scheme is different than the one used to control the single-switch converters that use unidirectional core excitation.

### 2.2.1 Flyback Converters

Flyback converters are derived from buck-boost converters. By adding a second winding to the inductor, electrical isolation is achieved. The topology is show in figure 2-7.

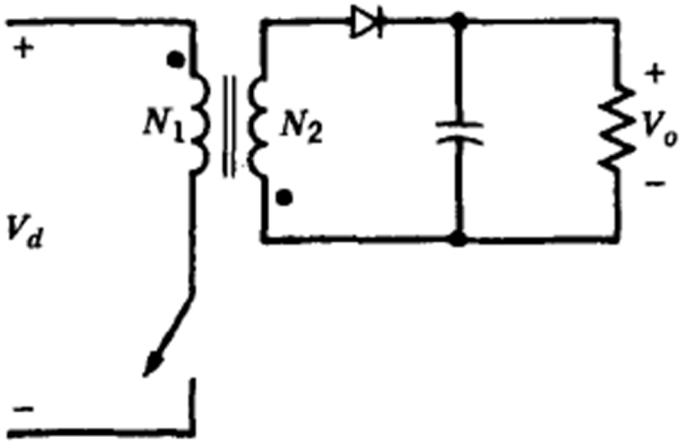


Figure 2-7: Flyback Converter [19].

The voltage transfer ratio in a flyback converter depends on the duty ratio in an identical manner as a buck-boost converter. The continuous-current-conduction mode in a buck-boost converter means that there is an incomplete demagnetization of the inductor core in the flyback converter. There are many variants of the flyback converter.

### 2.2.2 Forward Converters

Forward converters are derived from step-down converters. The voltage ratio in a forward converter is dependent on the duty ratio D in a similar manner to a step down converter. Figure 2-8 shows the circuit topology of a forward converter.

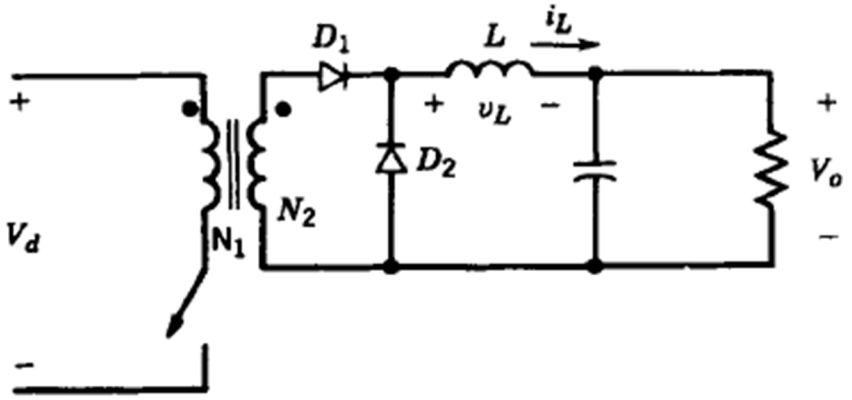


Figure 2-8: Forward Converter [19].

In practical, the transformer's magnetizing inductance should be included when analyzing and designing forward converters. The voltage transformation ratio $V_o/V_d$, however, is the same in either way. For the forward converter, there are many variant configurations.

### 2.2.3 Push-pull Converters

Push-pull converters are derived from step down conveters. The toplogy shown in figure 2-9 produces a sqaure wave ac signa at the input of the high frequency transformer. In this case, a center-tapped transformer is used which results in only one diode voltage drop on the secondary stage.

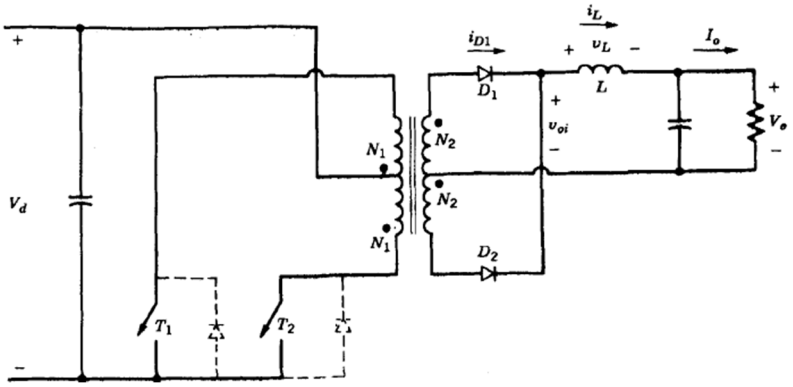


Figure 2-9: Push-pull Converter [19].

In push-pull converters, using a current-mode control scheme helps in eliminating the imbalance in the peak currents in the two switches T1 and T2.

### 2.2.4 Half Bridge Converters

Figure 2-10 shows an isolated half-bridge dc-dc converter. Only one switch is turned on at a time, but both switches can be turned off at the same time. Time 'Δ' corresponds to the interval where both switches are turned off. Regulating the output voltage is done by adjusting 'Δ'. The anti-parallel diodes with switches are used for protection.

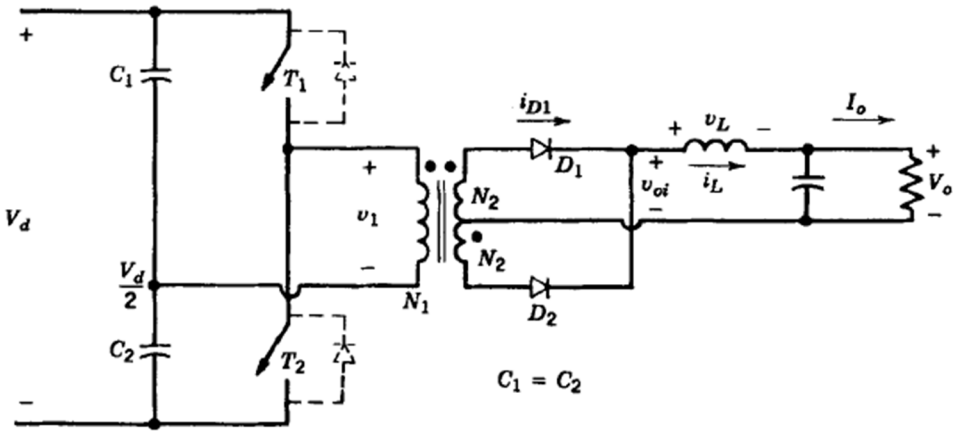


Figure 2-10: Isolated half-bridge converter [19].

### 2.2.5 Full Bridge Converters

Figure 2-11 shows an isolated full-bridge converter. Switches (T1, T2) and (T3, T4) are switched as pairs. This produces a high frequency square wave voltage signal at the input of the transformer (depends on the switching frequency). The center-tapped transformer and the two diodes at the secondary sides rectify the voltage to a DC voltage.

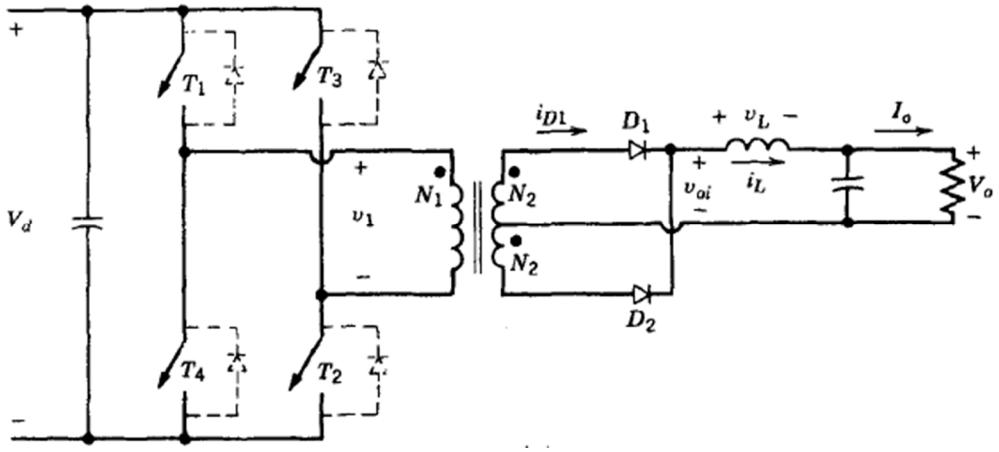


Figure 2-11: Isolated full-bridge converter [19].

Comparing the full bridge to the half bridge topology, for identical input voltage, output voltage and power rating:

$$\left(\frac{N_2}{N_1}\right)_{HB} = 2\left(\frac{N_2}{N_1}\right)_{FB}$$

If the ripple current at the output is neglected, and the magnetizing current is assumed to be negligible in both topologies, the switches currents compare as follows:

$$(\mathrm{I_{sw}})_{HB} = 2(\mathrm{I_{sw}})_{FB}$$

Therefore, in high power ratings it could be beneficial to use a full-bridge topology to have lower current going through the switches.

## 2.3 Series Resonant Converters

In switch-mode operation, the switches are subjected to high switching stresses and high switching power loss that increases linearly with the switching frequency of the PWM [9]. Large *dildt* and *dvldt* cause undesirable EMI, which is an additional drawback. Nevertheless, increasing the switching frequency is necessary to reduce converter size and weight, which increases the power density. These losses and stresses are minimized if the switching devices change state from on to off and off to on when their voltage (across) or the current (through) is zero at the instant of switching. Since most of these topologies (but not all) require some form of LC resonance, these are broadly classified as "resonant converters" [19]. The resonance concept and converter topologies that switch at ZVS and/or ZCS are discussed in this chapter.

Resonant converters are defined as the combination of converter topologies and switching strategies that result in zero-voltage and/or zero-current switching [19]. The addition of inductance $L_r$ and capacitance $C_r$ to the topology results in a resonant behavior. These elements comprise the resonant tank. Depending on how to wire these resonant elements in the resonant circuitry, two main classifications can inferred: series-loaded resonant converters (SLR) and parallel-loaded resonant converters (PLR). These converters are either half-bridge or full-bridge converters that have resonant tank (LC tank) added to them.

An LC tank is used in these converters, which causes the oscillation of the capacitor voltage and inductor current. This results in ZVS and/or ZCS. In the following analysis, only steady state is taken into account. The SLR converter act as a current source. As seen in

figure 2-12, the resonant capacitor and inductor are in series, and the resonant tank is in series with the load. This connection is the reason it's called a series loaded resonant converter. This is a full bridge topology. Half bridge option is also feasible; however, full bridge benefits from higher input voltage. A transformer is not necessary and the resonant tank can be connected directly to the rectifier bridge. A transformer provides electrical isolation and steps the voltage up or down if required by the specific application.

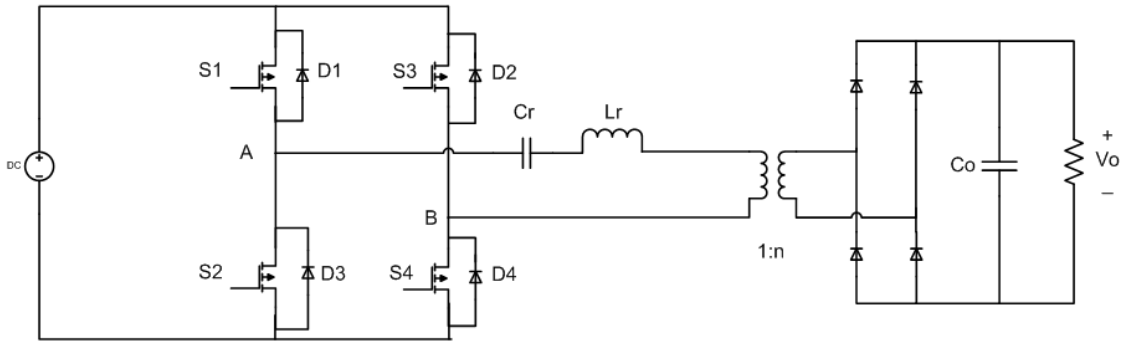


Figure 2-12: Series load resonant converter (SLR).

Figure 2-13 shows the equivalent circuit of the resonant converter. The reduction was made possible in this way due to the operation logic of the circuit. When switches S1 and S4 are conducting, $S_3$ and $S_4$ are off (assuming no phase shift) and $i_L$ is positive. When switches $S_2$ and $S_3$ are on, $S_1$ and $S_4$ are off, and $i_L$ is negative. Therefore, the voltage depends on the switch's state and direction of $i_L$.

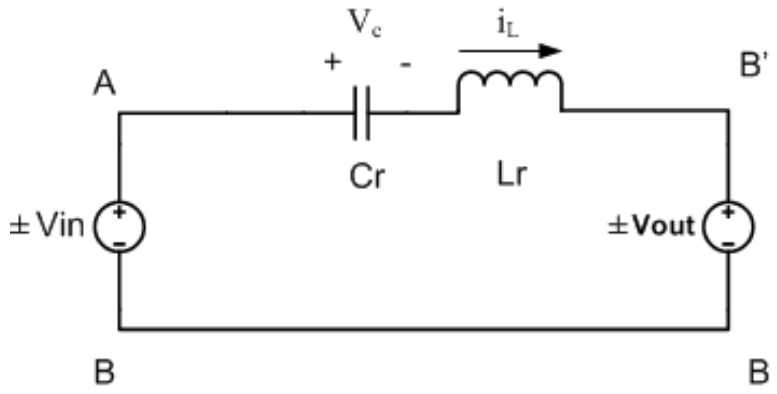


Figure 2-13: SLR equivalent circuit.

The positive half cycle occurs when switches $S_1$ and $S_4$ conduct, where the negative half cycle takes place when $S_2$ and $S_3$ conduct. The positive and negative half cycle are symmetrical since switches are operated in an identical manner. The repetition of these cycles and how fast it happens is determined by the switching frequency $f_s$ $(=w_s/2\pi)$. The switching frequency can be set to be above or below the resonant frequency $f_o(=w_o/2\pi)$, where $w_o=\frac{1}{\sqrt{L_r C_r}}$. This gives rise to three possible modes of operation based on the ratio of $f_s$ over $f_o$.

### 2.3.1 Discontinuous-Conduction Mode with $f_s<\frac{1}{2}f_o$

In this mode, operation of the converter (switching) is below the resonant frequency. This results in discontinuity in the inductor current as shown in figure 2-14. This is why it's called DCM mode. There are many advantages for operating in this mode. One big advantage is switches naturally turning off at zero current and zero voltage, since the inductor current goes to zero. Another advantage is better controllability over no load

conditions. One disadvantage is relatively higher conduction losses due to large peaks in the inductor current every cycle. These peaks occur since the switching frequency is relatively low, which allows the inductor current and capacitor voltage to fully resonate through a completer cycle.

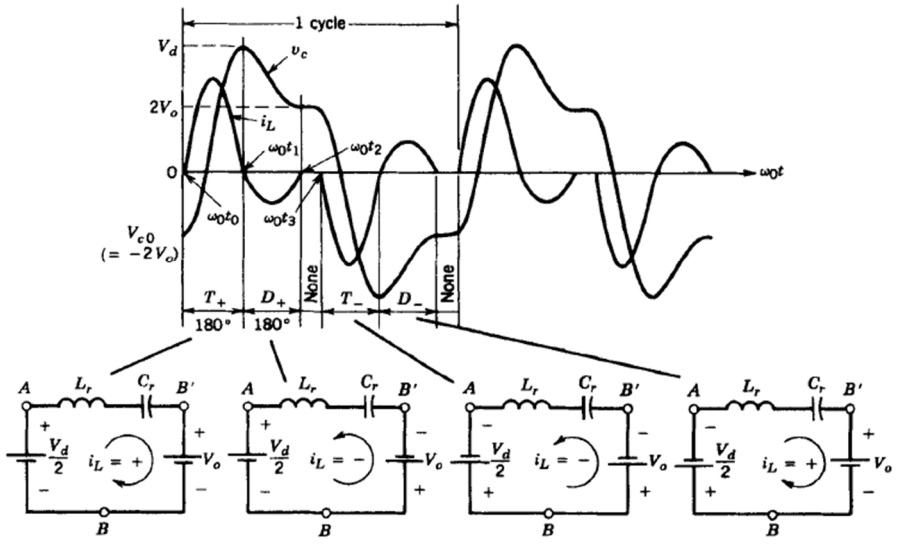


Figure 2-14: Discontinuous-conduction mode of operation SLR [19].

### 2.3.2 Continuous-Conduction Mode with $\frac{1}{2} f_o < f_s < f_o$

In this mode, operation is limited between half of the resonant frequency and the resonant frequency. In this mode of operation, the switches turn on at finite current and voltage, thus resulting in a turn-on switching loss [19]. However, this results in continuous inductor current. Turn off of switches occurs naturally at ZCS and ZVS in this mode. Diodes in this mode must have good revers-recovery characteristics.

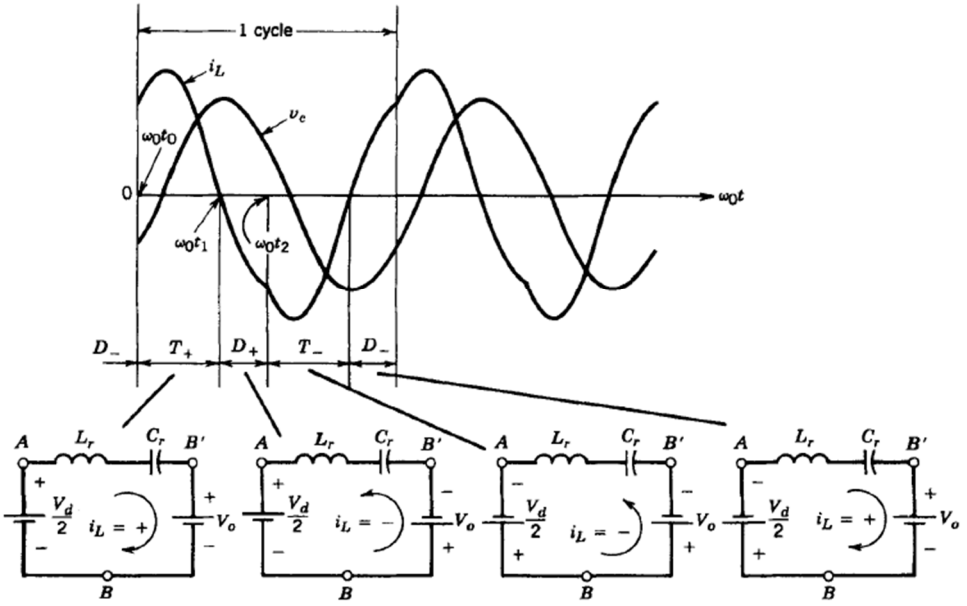


Figure 2-15: Continuous-conduction mode at sub-resonance for SLR [19].

### 2.3.3 Continuous-Conduction Mode with $f_s > f_o$

In this mode, operation is limited above the resonant frequency. Switches turn off at finite current, but turn on at a zero current and zero voltage. The current lags the voltage which guarantees ZCS turn on. Diodes in this range of operation do not need to have a very fast recovery due to turning on at ZVS and ZCS. However, turning off is near the peak of the inductor current as shown in figure 2-16, this is a disadvantage since it creates

significant turn-off switching loss. Lossless snubbers can be used in parallel with the switches to remedy this issue.

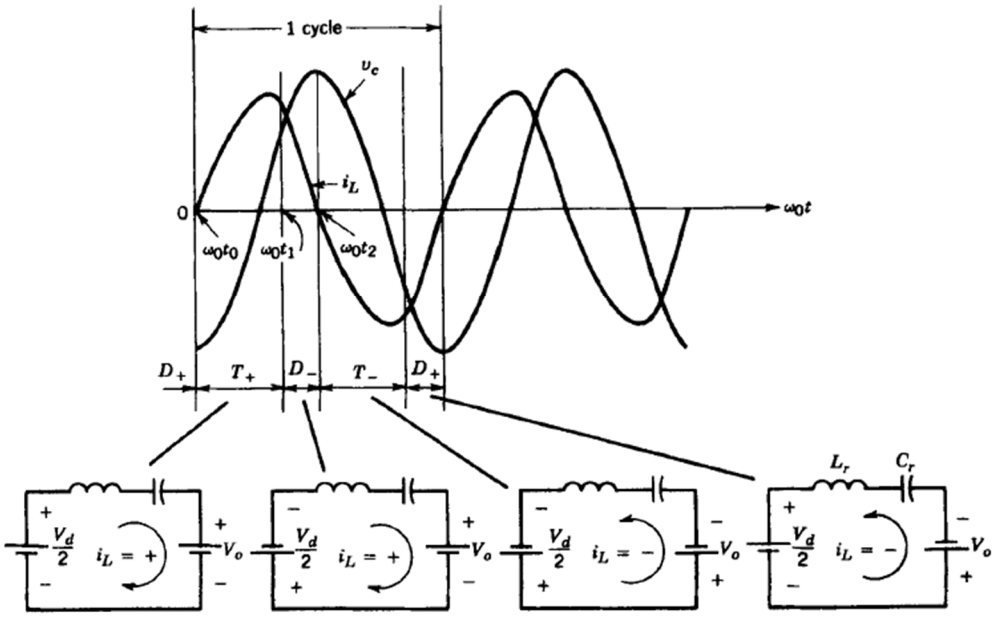


Figure 2-16: Continuous-conduction mode at super-resonance for SLR [19].

The output voltage in SLR converters can be regulated by changing the switching frequency $f_s$. As shown in figure 2-17, the normalized frequency $w_s/w_o$ determines the gain curve characteristics of the converter. SLR converters act as current sources. Looking at the figure, continuous conduction mode has the advantage of having larger gain for the converter, where the gain changes exponentially near the resonant frequency $w_o$.

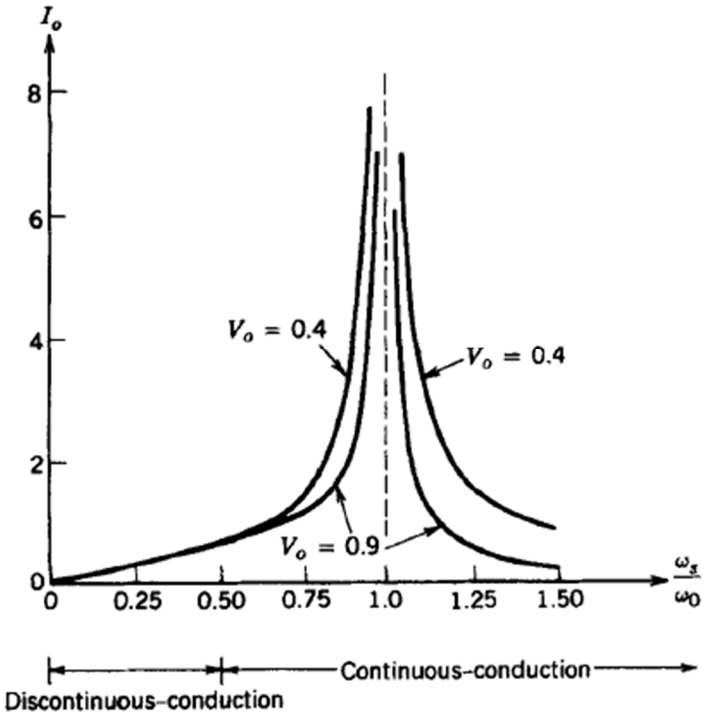


Figure 2-17: Steady-state characteristics of an SLR converter [19].

## 2.4 Parallel Resonant Converters

Parallel loaded resonant converters (PLR) are similar in operation to SLR converters. The resonant tank, however, appears in parallel with the resonant capacitor $C_r$, the topology is shown in figure 2-18. This type of converters are different from SLR converters in many aspects. PLR converters appear as voltage source and are better suited for multiple outlets [19]. PLR converters can step up or down the voltage, where SLR converters only operate

as step-down converters. One drawback for PLR converters is that they don't have inherent short-circuit protection like SLR converters.

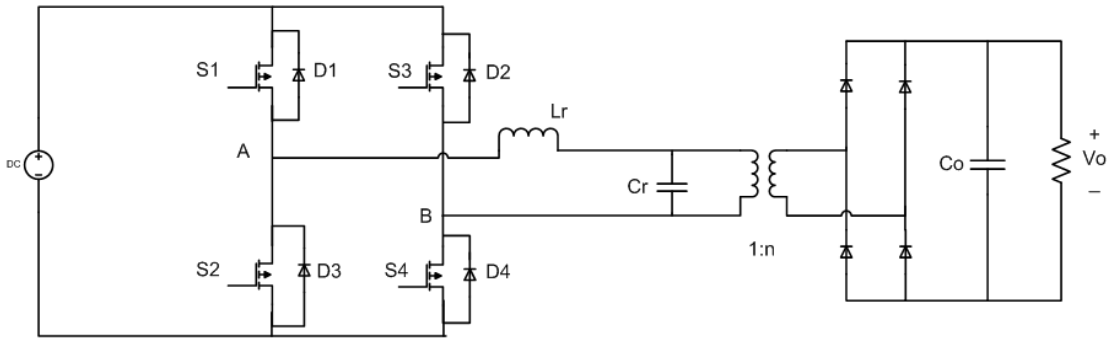


Figure 2-18: Parallel loaded resonant converter [19].

Figure 2-19 shows the equivalent circuit for PLR converters. The positive half cycle occurs when switches $S_1$ and $S_4$ conduct, where the negative half cycle takes place when $S_2$ and $S_3$ conduct. The positive and negative half cycle are symmetrical since switches are operated in an identical manner. This results in the "$\pm I_o$" seen at the terminals of the converters. PLR converters can operate in large number of combinations consisting of state of $i_L$ and $v_c$. Only three modes will be examined in the following sections.

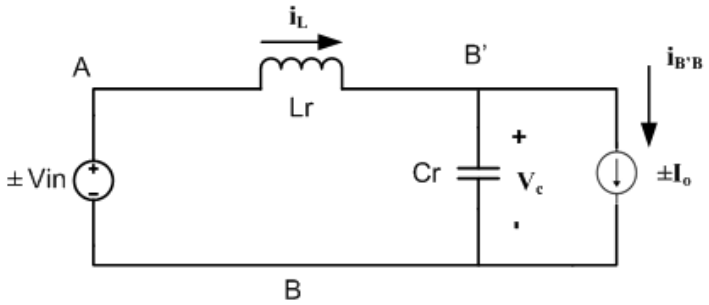


Figure 2-19: PLR equivalent circuit.

### 2.4.1 Discontinuous-conduction Mode with $f_s < \frac{1}{2} f_o$

This is the sub-resonant mode where the switching frequency is below the resonant frequency. Figure 2-20 shows the inductor current and capacitor voltage wavefroms in this mode. During deadtime, both $i_L$ and $v_c$ go and stay at zero. The output voltage can be controlled by varying this deadtime. This is also heplfull in adjusting for no load conditions. During the interval $t_0$ to $t_1$, the inductor current $i_L$ is less than output current $I_o$. Therefore, the output current circulates in the rectifier bridge and $C_r$ is shorted. In this mode of operation, there are no turn on or turn off losses on the switches.

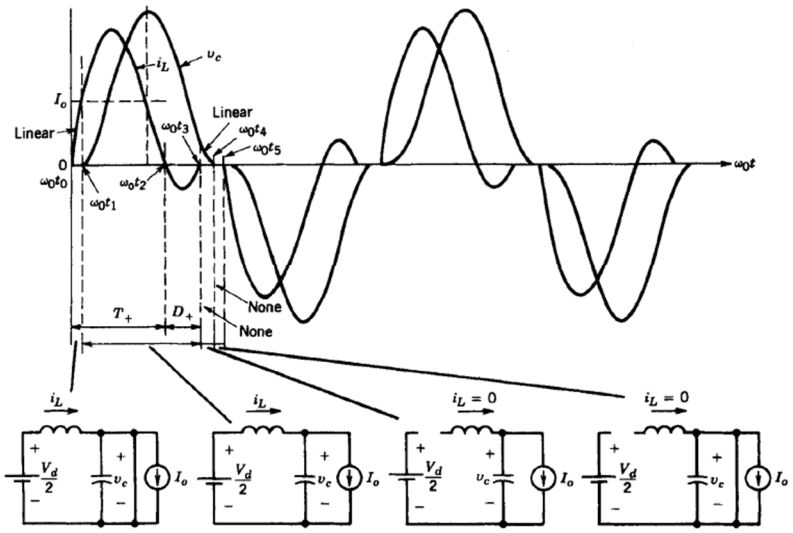


Figure 2-20: Discontinuous-conduction mode for PLR [19].

### 2.4.2 Continuous-Conduction Mode with $\frac{1}{2} f_o < f_s < f_o$

In this mode, switching frequency is higher than those in DCM mode but limited below the resonant frequency $f_o$. Switches turn on at a finite value of current, resulting in turn on loss. Diode, therefore, must have good reverse-recovery characteristics [19]. No turn off

losses in switches due to the natural commutation when $i_L$ reverses direction as show in figure 2-21.

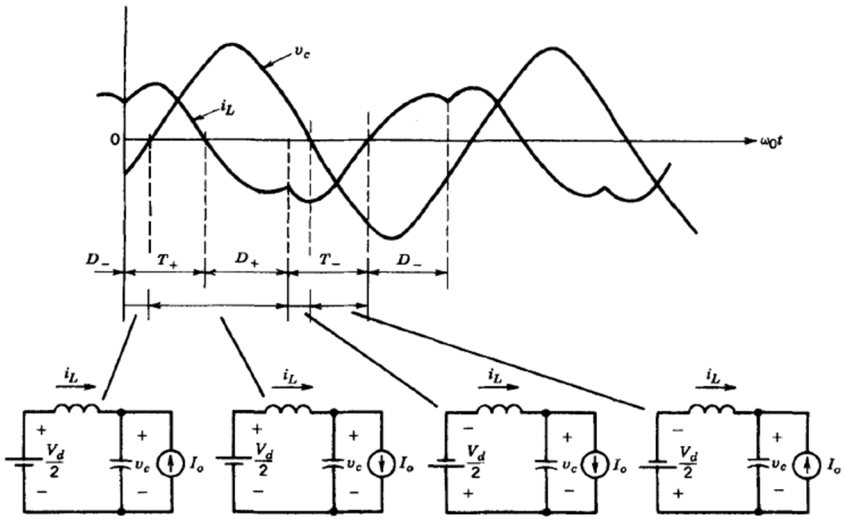


Figure 2-21: Continuous-conduction mode at sub-resonance for PLR [19].

### 2.4.3 Continuous-Conduction Mode with $f_s > f_o$

In this mode, operation is above the resonant frequency $f_o$ (super resonance).

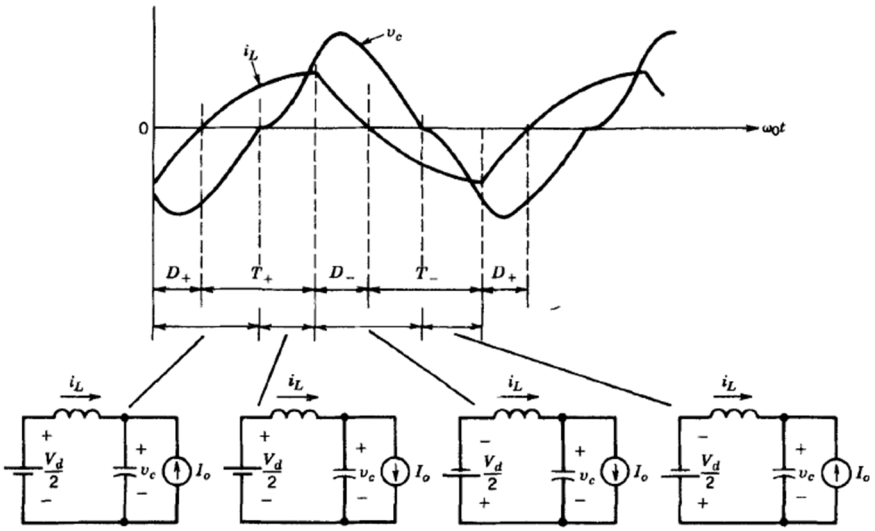


Figure 2-22: Continuous-conduction mode at super-resonance for PLR [19].

Turn on losses of the switches are eliminated to the natural commutation when $i_L$ reverses direction. Turn off losses, however, are present due to forcing the switch to turn off near the peak of the current. Similar to the SLR converter, turn on is at ZVS, and lossless turn off snubbers can be used in this case [19].

Once again, the output voltage can be regulated by changing the switching frequency $f_s$. PLR converters differ from their SLR counterparts in the fact that they act as a voltage source. Looking at figure 2-23, the converter has a good voltage characteristic in the DCM mode ($f_s < \frac{1}{2} f_o$), where the output voltage $V_o$ doesn't change as $I_o$ changes. This is a good property in designing converters with multiple outputs [19].

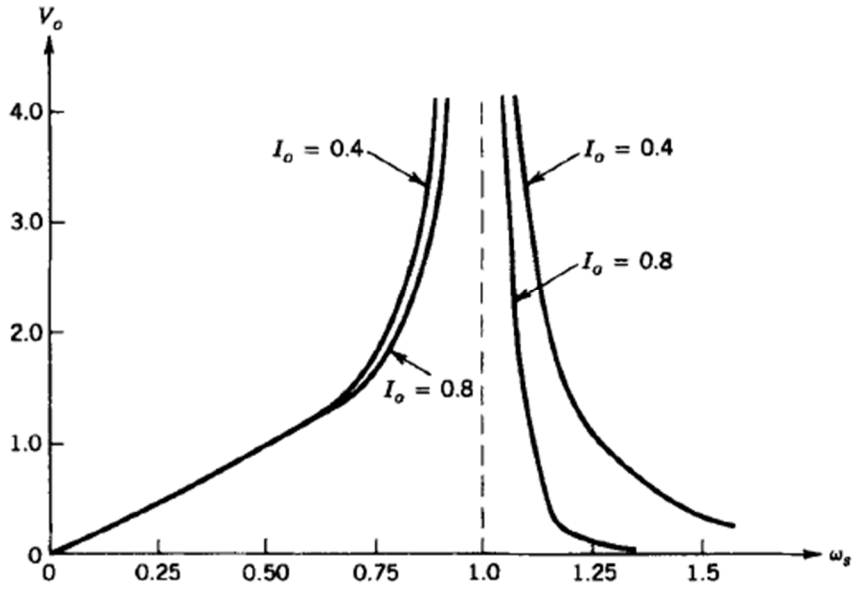


Figure 2-23: Steady-state characteristics of a PLR converter [19].

## 2.5 SST's and Microgrids

Micro-grids and distributed generation are the future of electricity generation and distribution. The technology behind wind turbines and solar panels is very saturated, and their market penetration is on the rise. Additionally, energy storage is gaining a lot of attention in research and several large corporates are investing in them. Revolutionizing energy storage will make the overall investment in renewables profitable and the R.O.E. achievable in reasonable number of years. However, to fully make the transition to distributed generation systems and micro-grids, there's a need of smart communication and controllability. Here is the importance of the so called *smart-grids*. Having that said, an SST provides the dynamics deemed crucial in such smart, versatile and modern systems. In this section, various types of solid state transformers are presented. The concept of microgrids is discussed and the justification of using SST's in microgrids is explained.

In 1968, William McMurray came up with the term - *Electronic Transformer* and later developed the *Thyristor Electronic Transformer*. According to William, the electronic transformer behaves in the same manner as a conventional power transformer in that it steps voltage levels up or down while providing isolation, and can accommodate load current of any power factor. It contained thyristor power switches which convert the low-frequency (dc to 400-Hz) voltage wave to a high-frequency (in the order of 10,000 Hz) wave. A comparatively small magnetic transformer then provides the voltage level transformation and isolation functions [20]. In 1980, J. C. Bowers et al, at the University of South Florida, described it as a *solid state transformer*, providing voltage regulation. It used

PWM AC power switching to achieve high efficiencies and used no large inductive components [21].

Transformers are fundamental components of the power distribution systems and are relatively inexpensive, highly reliable, and fairly efficient. However, they possess some undesirable properties including sensitivity to harmonics, voltage drop under load, (required) protection from system disruptions and overload protection of the system from problems arising at or beyond the transformer, environmental concerns regarding mineral oil, and performance under dc-offset load unbalances [1]. The concern is on the rise for these disadvantages as these would cause power quality issues especially in microgrid applications. Better quality for power can be achieved by using power circuitries, particularly with the advancement of power electronic circuits. Therefore, SST's can replace the conventional transformer that relies heavily on copper and iron.

Consequently, a big advantage that SST offers is the reduced volume and weight compared of the overall system compared to traditional transformers. SST's also offer several other advantages. It is insensitive to harmonics, prevents harmonics from propagating (in either direction), has zero regulation, prevents load disruptions and faults from affecting the primary system, can supply loads with dc offsets, and does not utilize a liquid dielectric. This allows for desirable advantages such as the power flow control, voltage sag compensation, fault current limitation, and etc., which are not possible for traditional transformers [21-23].

Smart grid technologies can deliver electricity from suppliers to consumers using digital technology with two-way communications to control appliances at consumer's

houses to save energy, reduce cost, increase reliability and transparency. A key characteristic difference compared to traditional grid network is the bidirectional flow for both power and information. Several demo micro-grid systems have been established in US, Europe, and Asia. Among them is the UWM microgrid and Future renewable electric energy delivery and management (FREEDM) center which are promising substitutions for future grid architecture. These systems are revolutionary power grids based on power electronics, high bandwidth digital communication, and distributed control.

A lot of research recently done is mainly focused on improving efficiency, reducing losses, realizing bidirectional power flow, enhancing power sharing, and providing efficient control methods at different voltage levels. A major problem for high voltage/ current applications of SSTs has always been the capacity of the semiconductor switches. The recent development Silicon-carbide (SiC) based semiconductors has helped with the advancement, and improvement of the voltage and thermal carrying capacity of SSTs. Doped Silicon has long been the semiconductor of choice in power electronics, but devices from SiC are faster, tougher, smaller in size and more efficient.

The bandgap of SiC devices, which is the energy needed to excite electrons from valence to conduction band, is the materials most attractive property. In such material, electrons need three times as much energy to reach the conduction band than their silicon counterparts. It is this property that lets SiC withstand high temperatures and voltages. Silicon devices cannot withstand voltages in excess of 300kV, but SiC are able to withstand voltages 10 times the maximum, with less than tenth the thickness of a silicon device. Making it faster, boasting less resistance, which means less energy is lost to heat during

conduction. SiC is used in semiconductor electronics devices that operate at high temperatures or high voltages, or both.

One area where SiC devices are already making inroads is solar power. Photovoltaic panels, whether they're mounted on a roof or spread across hectares of land, need inverters to convert the DC electricity made by the panels into AC electricity that can be fed into the power grid. Silicon carbide is a semiconductor in research and early mass-production. They are mature and inexpensive to manufacture, providing fast, high-temperature and/or high-voltage devices. The first devices available were Schottky diodes, followed by junction-gate FETs and MOSFETs for high-power switching. Bipolar transistors and thyristors are currently developed

To fully answer the question of where SST's fit in a Smart grid, a comparison of SST's to conventional transformers is presented below:

| **Conventional Transformer** | |
|---|---|
| **Pros** | **Cons** |
| • Relatively inexpensive. | • Voltage drop under load. |
| • Highly robust and reliable. | • Losses at no load. |
| • Highly efficient. | • Weight. |
| • Short circuit current limitation. | • Construction volume. |
| | • Sensitivity to harmonics. |
| | • Sensitivity to DC offset load imbalances. |
| | • No overload protection. |
| | • Possible fire hazard. |
| | • Environmental concerns. |

Table 2: Conventional transformer pros and cons.

| SST | |
|---|---|
| **Pros** | **Cons** |
| • Full control of power flow. | • Voltage breakdown of typical semiconductor components may be problematic.<br>-Resolved through use of more suitable semiconductor materials or voltage limiting devices. |
| • Power factor control. | • High power switching losses proportional to switching frequency.<br>-Resolved through Zero voltage and current switching technology. |
| • Reduction in size. | • No ohmic isolation offered by semiconductor switches.<br>-Resolved by the use of a magnetic transformer. |
| • Assists in the integration of Distributed Energy Resources. | • Loss of life and performance issues due to heat.<br>-Resolved by using better cooling and packaging schemes. |
| • Assists in the integration of Distributed Energy Storage. | |
| • Protects power system from load disturbances. | |
| • Protects load from power system disturbances. | |
| • Enables distribution integration through communication. | |
| • Ensures stability and optimal operation. | |

Table 3: Solid state transformer pros and cons.

# CHAPTER III

## 3. LLC RESONANT SST

### 3.1 Mathematical Analysis

The LLC resonant network acts as filter for the square wave voltage seen at the terminals of the full-bridge converter. This results in a pseudo sinusoidal current seen at the primary side of the transformer. In most common modes of operation, the controlled switch network produces a square wave voltage output $V_d$ whose frequency is close to the tank network resonant frequency. The tank output waveform is then rectified to produce the dc load voltage $V_o$. By changing the switching frequency $f_s$, the magnitude of the tank ringing response can be modified to change the dc output voltage. In this case, the resonant tank responds primarily to the fundamental component $f_s$ of the switch waveform $V_s$, and has negligible response at the harmonic frequencies n*$fs$, n=3, 5, 7 … [24].

First Harmonic Approximation (FHA) is used here to obtain the transfer function that describes the gain of the resonant network. Figure 3-1 shows the resulting equivalent circuit.

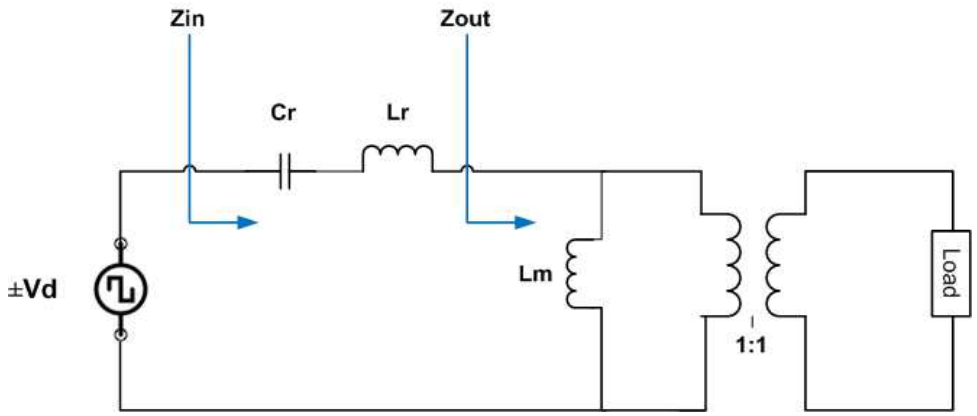


Figure 3-1: LLC Resonant converter using FHA analysis.

The input of the resonant network is a square wave varying between $-V_d$ and $V_d$. Using Fourier series, the input voltage can be expressed by equation (1) [4].

$$v_d(t) = \frac{4V_d}{\pi} \sum_{n=1,3,5,\dots}^{\infty} \frac{1}{n} \sin(2\pi n f_s t) \tag{1}$$

Where $f_s$ is the switching frequency of the switches in the resonant network. The fundamental component of $v_d(t)$ can be obtained using the FHA analysis. The fundamental component, $v_{d,FHA}(t)$, is then can be obtained as:

$$v_{d,FHA} = \frac{2\sqrt{2}}{\pi} V_d \tag{2}$$

Equation (2) does not take into account a varying phase shift between the two legs of the inverter. If this phase shift is represented by angle '$\alpha$', the output voltage of the inverter can be described as:

$$(V_o)_h = \frac{4}{\pi h} V_d cos(\frac{1}{2}\alpha) \tag{3}$$

The effective output load resistance seen in parallel with the magnetizing inductance $L_m$ is defined as $R_e$. This accounts for the turn's ratio of the transformer and the output load. Using FHA allows writing $R_e$ as follows:

$$\mathrm{R_e} = \frac{8}{\pi^2}\mathrm{R_o} \tag{4}$$

The transfer function of the resonant network, defined as the ratio of the output voltage over the input voltage is then:

$$\mathrm{H_r} = \frac{\mathrm{V_{o,FHA}}}{\mathrm{V_{d,FHA}}} = \frac{\frac{\mathbf{sL_m * R_e}}{\mathbf{sL_m + R_e}}}{\mathbf{(sC_r)^{-1} + sL_r + \frac{sL_m * R_e}{sL_m + R_e}}} \tag{5}$$

Now, the normalized frequency "$f_n$" can be written in terms of the switching frequency "$f_s$" and the first resonant frequency "$f_r$" as follows:

$$\mathrm{f_n} = \frac{\mathrm{f_s}}{\mathrm{f_{r1}}} \tag{6}$$

Where $f_{r1} = \frac{1}{2\pi\sqrt{L_r C_r}}$

There is also a second resonant frequency shown in figure 3-2, this is a resultant of both inductances *Lm* and *Lr* combined.

$$f_{r2} = \frac{1}{2\pi\sqrt{(L_r + L_m)C_r}} \tag{7}$$

The quality factor "Q" and the inductance ratio "k" are given by:

$$\mathrm{Q} = \frac{\mathrm{Z_r}}{\mathrm{R_e}}; \quad \mathrm{Z_r} = \sqrt{\frac{\mathrm{L_r}}{\mathrm{C_r}}}; \quad \mathrm{k} = \frac{\mathrm{L_r}}{\mathrm{L_m}} \tag{8}$$

Using the above terms, $H_r$ can be reformulated as follows:

$$H_r = \frac{\frac{jf_n}{k}}{\left[\frac{Q}{k} - \frac{f_n^2 Q}{k}\right] + j\left[f_n + \frac{f_n}{k} - \frac{1}{f_n}\right]} \quad (9)$$

The magnitude of $H_r$ is obtained and evaluated at ($j2\pi f_s$) as follows:

$$|H_r| = \left| \frac{\frac{jf_n}{k}}{\left[\frac{Q}{k} - \frac{f_n^2 Q}{k}\right] + j\left[f_n + \frac{f_n}{k} - \frac{1}{f_n}\right]} \right| \quad (10)$$

Equation (10) describes the gain of the SST as a function of several important parameters: fn, Q and K. This equation describes the gain Vout/Vin. A plot of the gain curve described by equation (10) is shown figure 3-2. This plot, however, assumes a fixed duty cycle of the switches the produces a perfect square wave at the input of the resonant tank as shown in figure 3-1. If equation (3) is to be taken into account, then the gain curve will vary according to the value of the phase shift $\alpha$, which dictates the duration of the duty cycle. Figure 3-3 shows the gain curve plotted at two different values of $\alpha$.

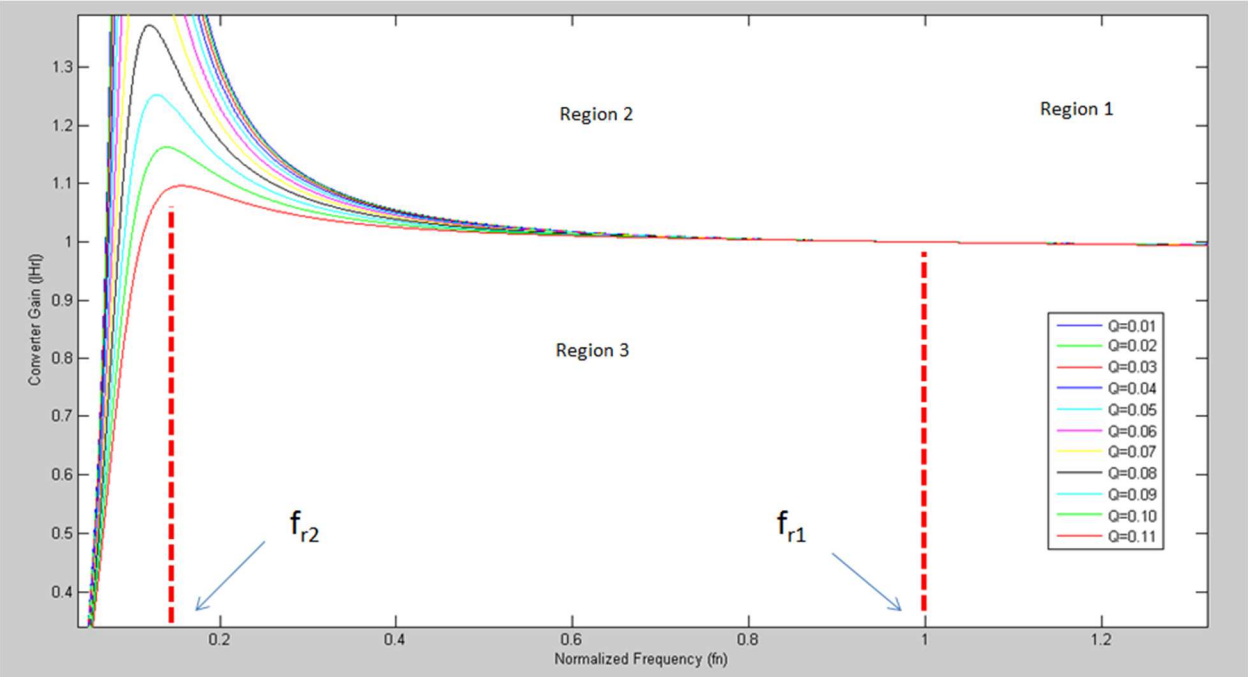


Figure 3-2: Resonant converter gain plot versus normalized frequency at various values of Q at a fixed duty cycle.

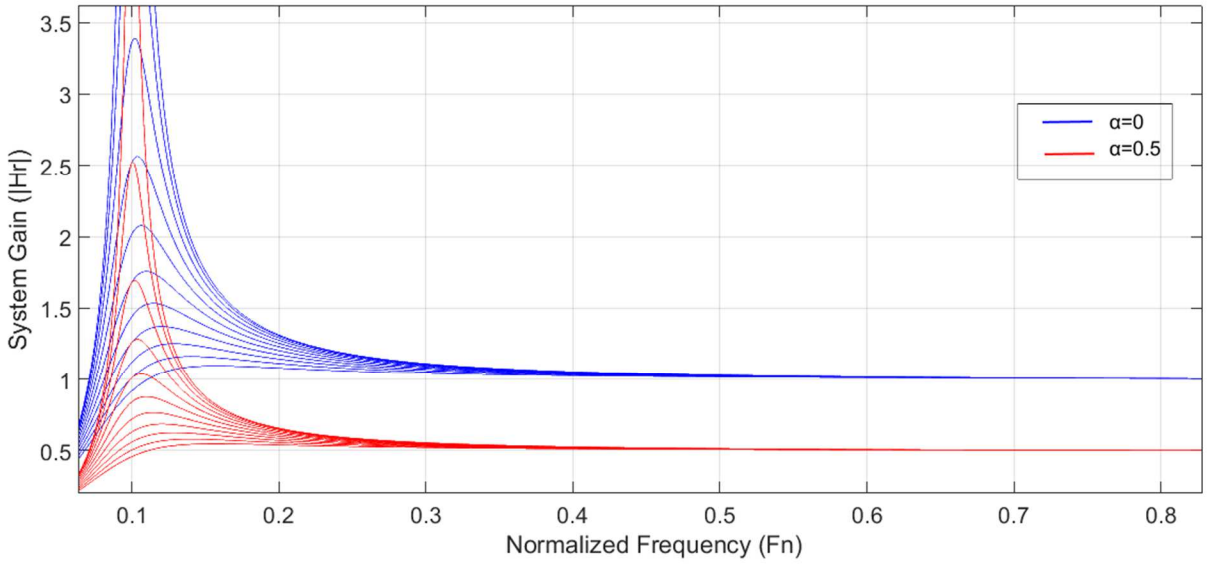


Figure 3-3: Gain at two different phase-shift values ($\alpha$).

As defined in equation (8), Q takes into account the load $R_e$. Thus, plotting versus many values of Q calculates how the gain of the converter's gain would change and behave under no load or over load conditions. In figure 3-2, three regions of operation are defined as region 1, region 2 and region 3. Region 1 corresponds to operation above $fr_1$ and it's the super-resonance region. The magnetizing inductance does not participate in resonance and ZVS is naturally assured [8]. Region 2 is the multi-resonant converter (MRC) region. Depending on the load, converter could operate either in ZVS or ZCS. Region 2 is the light load region where the converter operates in ZVS. In this region, the energy stored in the magnetic components causes ZVS for the opposite switching device [8]. Region 3 is the heavy load region where the converter operates in ZCS mode [8]. The magnetizing inductance Lm determines the amount of switch off current. The smaller the value of Lm is, the higher the switch off current on the switching devices, which causes losses and stresses.

In this research, the focus is on switching in the super-resonance region. In order to maintain a regulated voltage on the output that accounts for a varying load, fs has to change in a wide range as shown in figure 3-2. Using phase shifting, canceling part of the duty ration makes it possible to reduce the gain of the converter and hence regulate on a narrower fs range. Therefore, this is better in handling a no load condition.

### 3.2 Gain Curve Analysis:

Looking at figure 3-2, there are two resonant frequencies $f_{r1}$ and $f_{r2}$ that are the result of $L_r$ and the combined inductances $L_r$ and $L_m$, respectively. The gain of the resonant

converter has to be monotonically decreasing within the operating frequency range. Taking the derivative of eq. (10) and setting it to less than zero, the following inequality is obtained:

$$Q < \sqrt{\frac{B(f_n)}{A(f_n)}} \tag{11}$$

; Where $A(f_n)$ and $B(f_n)$ are given as follows:

$$A(f_n) = f_n^4\left(\frac{-1}{2k^2}\right) + f_n^2\left(\frac{-1}{k}\right) + \frac{1}{k^2} \tag{12}$$

$$B(f_n) = f_n^2\left(\frac{1}{k^2} + \frac{2}{k} - \frac{3k}{2} + \frac{1}{2}\right) + \left(\frac{-2-2k}{k}\right) + \frac{3}{2f_n^2} \tag{13}$$

$R_o$ can be expressed as a function of the output voltage and output current. Using the condition obtained in (11), a condition for the maximum load current, $I_{o,max}$, can be derived as follows:

$$I_{o,max} < \frac{8V_oQ_{max}}{\pi^2 Z_r} \tag{14}$$

Alternatively, a condition for maximum $Z_r$ at a given $I_{o,max}$ can be derived:

$$Z_r < \frac{8V_oQ_{max}}{\pi^2 I_{o,max}} \tag{15}$$

### 3.3 Soft Switching Analysis:

Switching at high frequency increases losses, stresses and electromagnetic interference across the switching devices. This could be deteriorating to the switches at some switching frequencies and power rating, which requires the use of techniques that reduce stresses across the switches upon switching. Figure 3-4 shows the waveforms for

hard switching. In figure 3-4(a), switch on and switch off transients are shown. A finite value of voltage and current is present across the switch, and gets dissipated at losses. This also causes stresses and ringing across the switch, which is more severe with higher switching frequencies. Figure 3-4(b) shows the switching on and off trajectory. $I_0$ is the current being conducted by the switch when it's turned on, where $V_d$ is the voltage across the switch when it's turned off. The whole area under these lines is the amount of power dissipation.

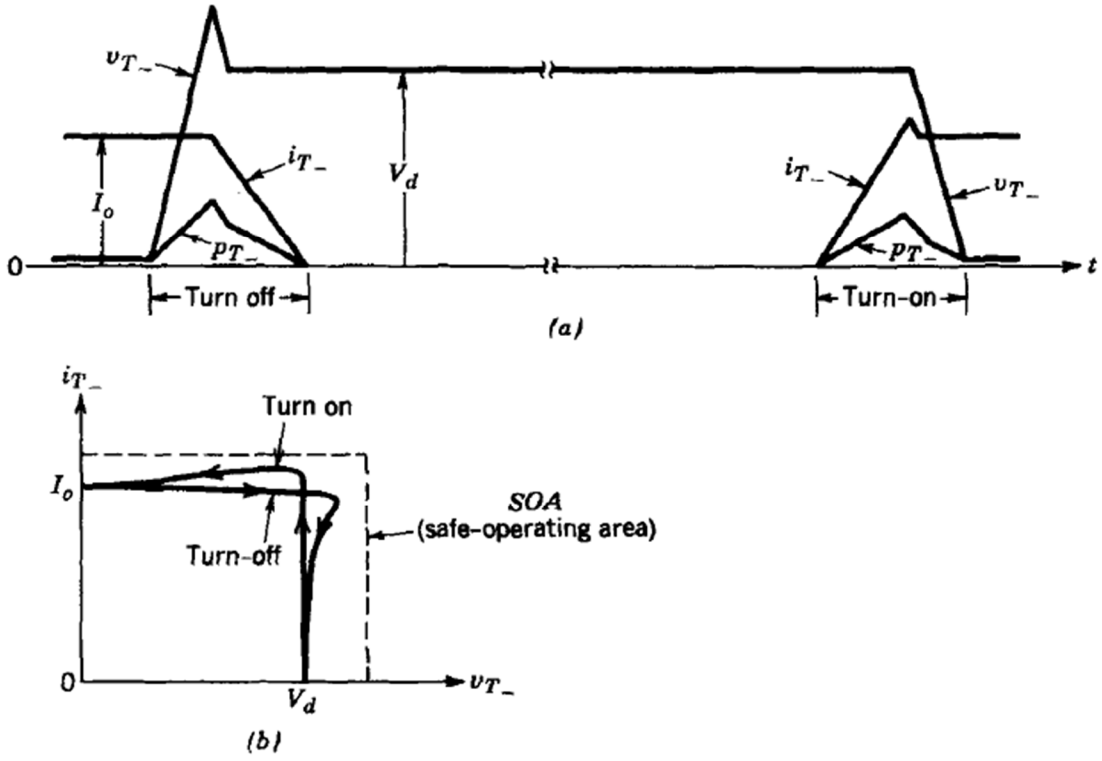


Figure 3-4: Hard switching waveforms: (a) Current and voltage waveforms (b) Switching trajectory [19].

Figure 3-5 shows the switching trajectories of the device using a snubber circuit. Looking at the area under the lines, the power dissipation is reduces significantly.

Therefore, switching stresses and EMI is reduced. This essentially permits operating at higher switching frequency and/or power ratings.

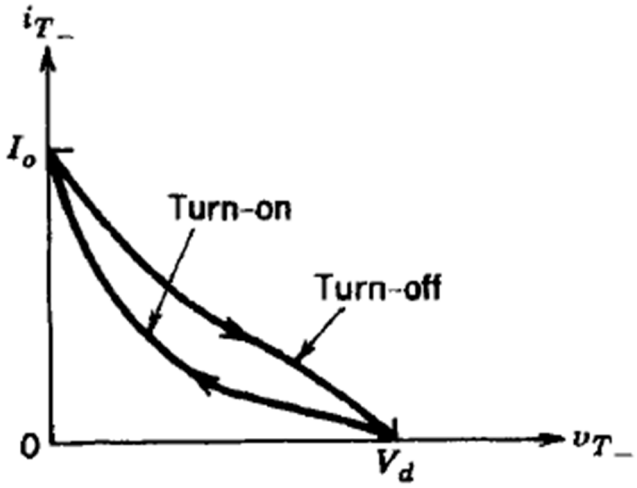


Figure 3-5: Switching trajectory with a snubber circuit [19].

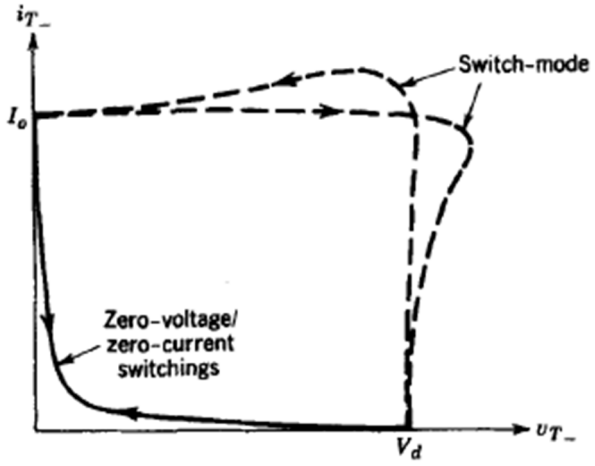


Figure 3-6: Switching trajectory with ZVS/ZCS switching [19].

For all switches, ZVS at turn on is very important to minimize losses and stresses. In figure 3-7(b), when only $S_1$ is turned ON, the output capacitance of $S_3$ is being discharged in preparation for ZVS turn-on, while the output capacitance of $S_4$ is being charged. This underlines a condition to ensure ZVS operation: the primary current discharges the

capacitances of the switches for turning on at ZVS. Therefore, the minimum dead-time duration is described as:

$$\mathrm{t_d} \geq \frac{\mathrm{V_d C_{switch}}}{\mathrm{i_p}} = 4\mathrm{C_{switch} f_s L_m} \tag{16}$$

$C_{switch}$ stands for the capacitance connected across both switches in the leading leg, $i_p$ stands for the primary current, and $f_s$ stands for the maximum switching frequency. So, $L_m$ is limited by:

$$L_m \leq \frac{t_d}{4C_{switch} f_s} \tag{17}$$

For the switches on the lagging leg (S3 and S4), ZVS turn off is very important for minimizing losses and stress. This can be achieved with the help of a snubber circuit. Having the maximum operating frequency specified, and taking into account the maximum magnetizing inductance $L_m$, the maximum possible capacitance that can be used at which the time constant for the capacitor discharge is less than the minimum half period at no load is [25]:

$$\mathrm{C_{snubber-max}} = \frac{1}{\mathrm{L_m}(2\pi \mathrm{f})^2} \tag{18}$$

As for ZCS, the freewheeling state created by phase shifting both legs of the H-bridge brings the resonant current almost to zero. The freewheeling state is shown in figure 3-7(b-c) for the positive half cycle, and figure 3-7(f-g) for the negative half cycle. Therefore, the leading leg (S1 and S2) benefit from ZCS. A minimum phase shift ($\alpha$) is specified in the controller to ensure enough freewheeling time to bring the current to as close to zero.

### 3.4 Circuit Operation:

The proposed resonant converter is operated using Pulse Frequency Modulation (PFM) and Phase Shift Modulation (PSM). It is operated by turning off one set of the H-bridge leg earlier than the other set. The imposed phase shift between the two legs creates three different levels on the output of the inverter: $V_i$, - $V_i$, and 0. Thus, there is a discontinuity in the current every half period, which results in DCM operation at super resonant frequency. From a power transfer point of view, the amount of current being delivered by the converter to the output dictates the amount of the delivered power. Therefore, there are two parameters that control the power flow: switching frequency (fs) and phase shift ($\alpha$). Looking at figure 3-3, a range of combinations of fs and $\alpha$ are all possible points of operation. This is extremely helpful in adjusting to no load or low load conditions at super resonance.

The modes of operation are shown in figure 4. Modes 1 and 5 are both powering modes, corresponding to the positive half cycle and the negative half cycle, respectively. Modes 2 through 4 repeat after Mode 5 to undergo the same transition for the left leg. The leading leg in this topology (leg that turns off first) is the leg that contains switches $S_3$ and $S_4$.

*Mode 1:* This mode starts by turning on $S_4$ and $S_1$. The primary current $i_d$ and inductor current $i_{Lr}$ begin to increase. The secondary voltage is reflected through the transformer. The magnetizing inductance does not resonate in this mode; its magnetic energy is built up linearly due the presence of the output voltage across its terminals.

The equations of the primary current and capacitor voltage are:

$$i_L(t) = i_L(t_1)\cos\big(w_{r1}(t-t_1)\big) + \big(V_{dc} - V_0 - v_c(t_1)\big)\sqrt{\frac{C_r}{L_r}}\ \sin(w_{r1}(t-t_1)) \quad (19)$$

$$v_c(t) = V_{dc} - V_o + (V_{dc} - V_o + v_c(t_1))\cos(w_{r1}(t-t_1)) + i_L(t_3)\sqrt{\frac{L_r}{C_r}}\sin(w_{r1}(t-t_1)) \quad (20)$$

Where $w_{r1} = \frac{1}{\sqrt{L_r C_r}}$

*Mode 2:* This mode starts by turning $S_4$ in the leading leg (leg that contains $S_3$ and $S_4$) off. A freewheel state will start where the resonant current will go through $D_3$ and $S_1$. Therefore, the output of the inverter becomes zero. This mode limits the output power during low-load. The magnetizing inductor still sees the output voltage across its terminals,$V_m = -V_o$, which keeps the output diodes forward biased. The respective equations for this mode are found to be:

$$i_L(t) = i_L(t_2)\cos\big(w_{r1}(t-t_2)\big) + (V_0 - V_{dc})\sqrt{\frac{C_r}{L_r}}\ \sin(w_{r1}(t-t_2)) \quad (21)$$

$$v_c(t) = -V_{dc} + V_o + (V_{dc} - V_o + v_c(t_2))\cos(w_{r1}(t-t_2)) + i_L(t_2)\sqrt{\frac{L_r}{C_r}}\sin(w_{r1}(t-t_2)) \quad (22)$$

This mode ends when the resonant current across $L_r$ becomes equal to the magnetizing current across $L_m$, thus the output diode current is zero implying that these diodes are turned off.

*Mode 3:* In this mode, the magnetizing inductor participates in the resonant behavior with $L_r$ and $C_r$, where the output is separated from the transformer and does no contribution to the energy flow.

$$i_L(t) = i_m(t) = i_L(t_3)\cos\big(w_{r2}(t-t_3)\big) - (V_c(t_3))\sqrt{\frac{C_r}{L_r+L_m}}\ \sin(w_{r1}(t-t_2)) \quad (23)$$

$$v_c(t) = v_c(t_5)\cos(w_{r2}(t-t_1)) + i_L(t_5)\sqrt{\frac{L_r+L_m}{C_r}}\sin(w_{r2}(t-t_5)) \quad (24)$$

Where $w_{r1} = \frac{1}{\sqrt{(L_m+L_r)C_r}}$.

*Mode 4:* This mode is a "dead time" mode. All switches $S_1$ through $S_4$ are turned off to guarantee safe operation when the next pair of switches is ready to be turned on [25].

*Modes 5 through 8:* In these modes, similar behavior to modes 1 through 4 repeats, but the transition here starts with turning S3 off. These modes correspond to the negative half-cycle of the inverter, whereas modes 1 through 4 correspond to its positive half cycle.

The design aims to insure ZVS and/or ZCS operation of the converter at different load conditions. The converter is operated under varying switching frequency and phase shift between the legs of the H-bridge. This results in ZCS for the lagging leg across full load range. As for the leading leg, ZVS operation will be analyzed.

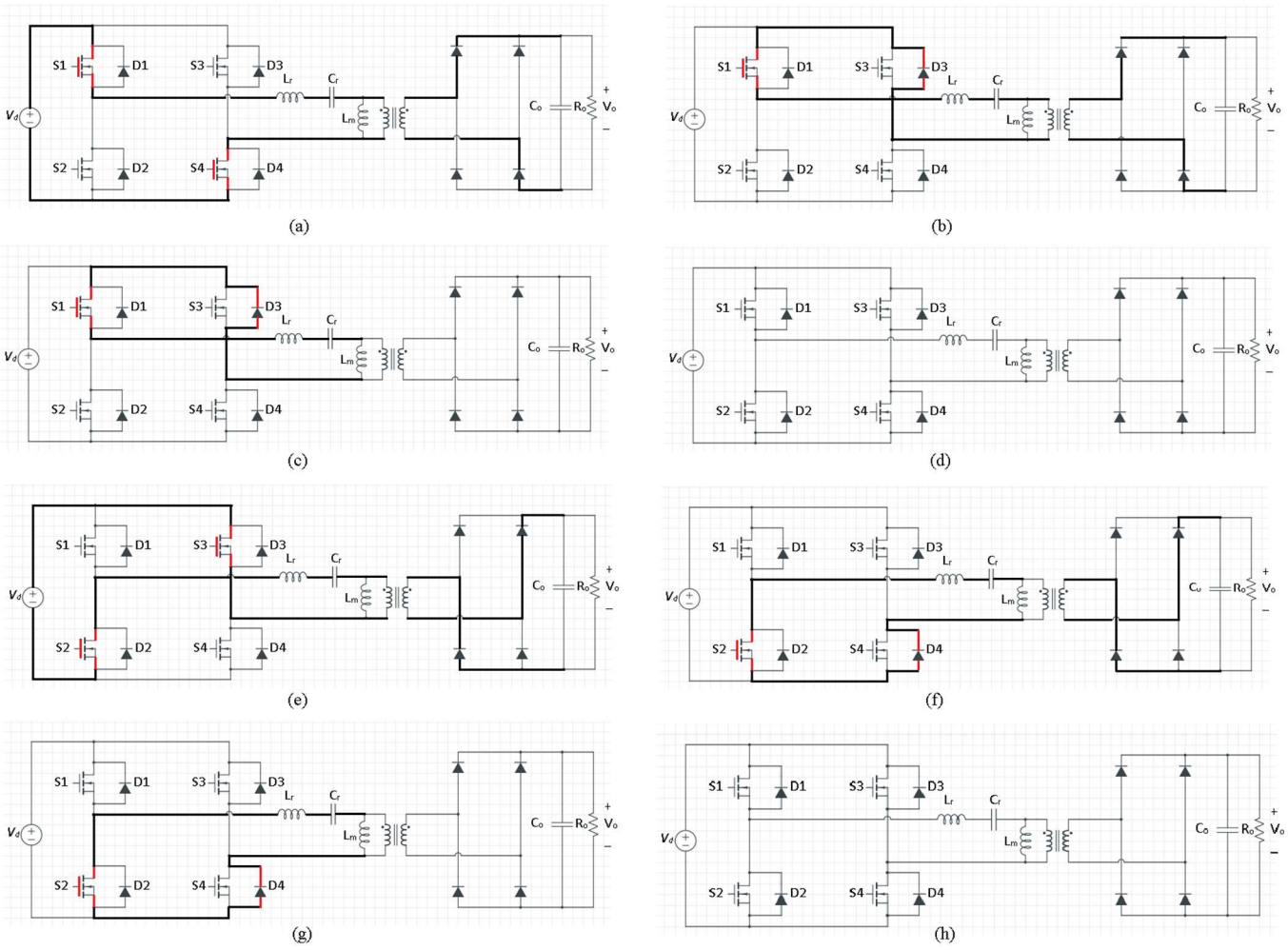


Figure 3-7: Operation Modes of the series resonant converter: (a) Mode 1, (b) Mode 2, (c) Mode 3, (d) Mode 4, (e) Mode 5, (f) Mode 6, (g) Mode 7 (h) Mode 8.

# CHAPTER IV

## 4. CONTROLS

It is extremely important to maintain a regulated output DC voltage to support a varying load requirement. This is one of the main problems tackled in this research. A combination of two control schemes, PSM and PFM, is utilized to control the converter. PFM stands for pulse frequency modulation and PSM stands for phase shifting modulation.

### 4.1 PFM and PSM Control Scheme:

PFM is applied by varying the switching frequency "*fs*" to adjust the point of operation on the gain curve (figure 3-3). PSM is then implemented by adjusting the duty ratio of $S_3$ and $S_4$ in order to increase or decrease the overlap between the two leg's phase voltages. This overlap, described as the angle $\alpha$, corresponds to a zero state (zero voltage) at seen at the terminals of the inverter.

Using both PFM and PSM, it is possible to support a wider range of load [25]. Adjusting duty cycle enables holding to a specific switching frequency for a varying load. Alternately, the converter can be operated at lower switching frequencies for lower duty cycles for a fixed load. Figure 4-1 shows a plot of fs vs duty ratio for two different load requirements that are fixed at 18A and 20A. In this case, decreasing both fs and duty ratio permits the controller to support a fixed load requirement, and regulate a specific desired voltage level. Figure 4-1 shows that a wider range of output voltage is realized when using both PFM and PSM. Conventionally, a converter that uses PFM would have a fixed gain curve

(for a fixed load). In figure 4-2, the whole dotted area between the upper and the lower curves that correspond to duty ratio of 1 and 0.1 represents possible points of operation.

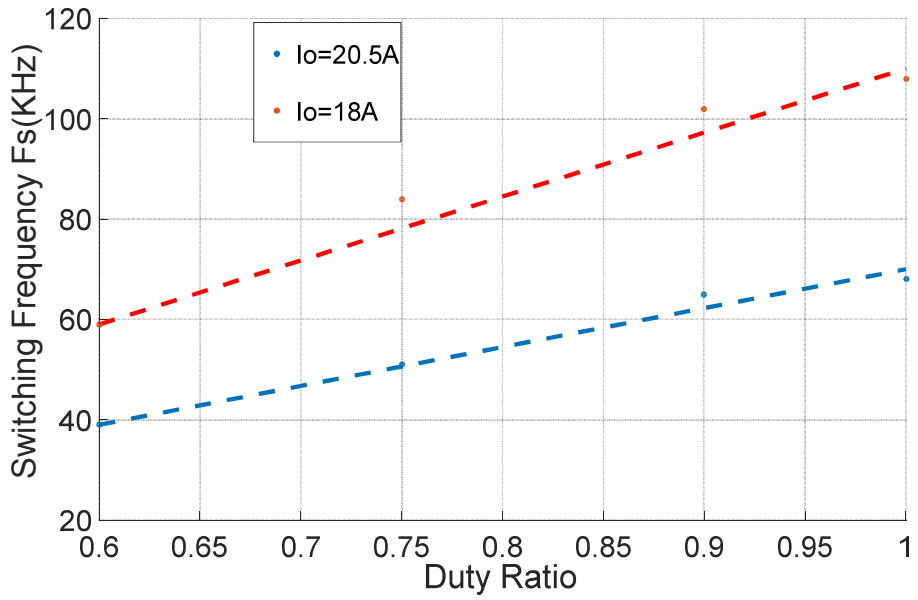


Figure 4-1: Switching frequency versus duty ratio.

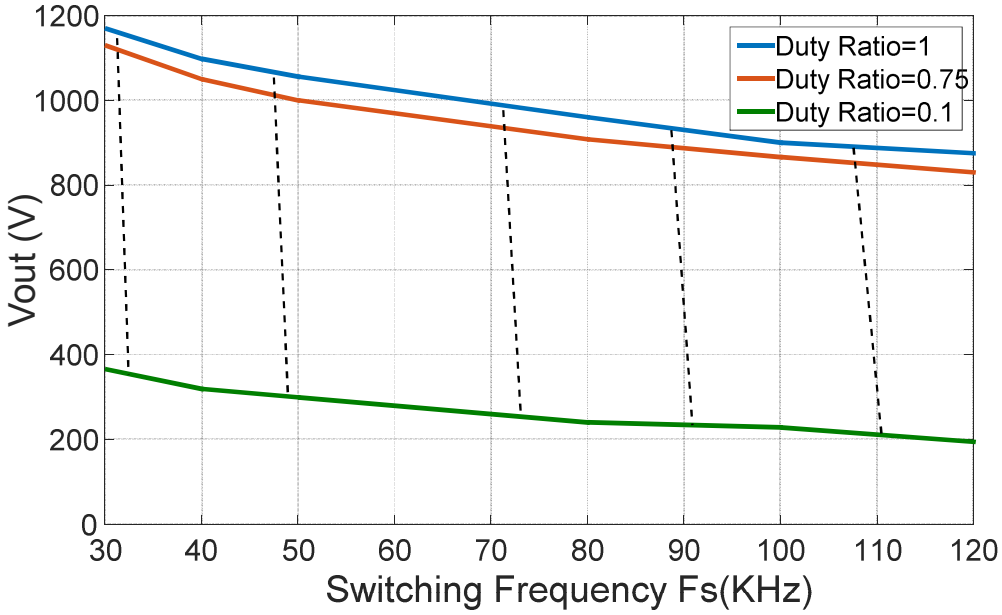


Figure 4-2: Vout at a different duty ratios for a spectrum of fs.

Figure 4-3 shows the block diagram of the proposed controller. The voltage on the output is regulated by adjusting the resonant current. The resonant is controlled by adjusting the switching frequency fs and the phase shift α. The leftmost PI block in figure 4-3 calculates the next switching frequency based on the error on the output voltage. The rightmost PI block calculates the required phase shift angle α required to drive this switching frequency to the desired reference. With α varying, the switching frequency $f_s$ keeps on updating until it reaches $f_{ref}$.

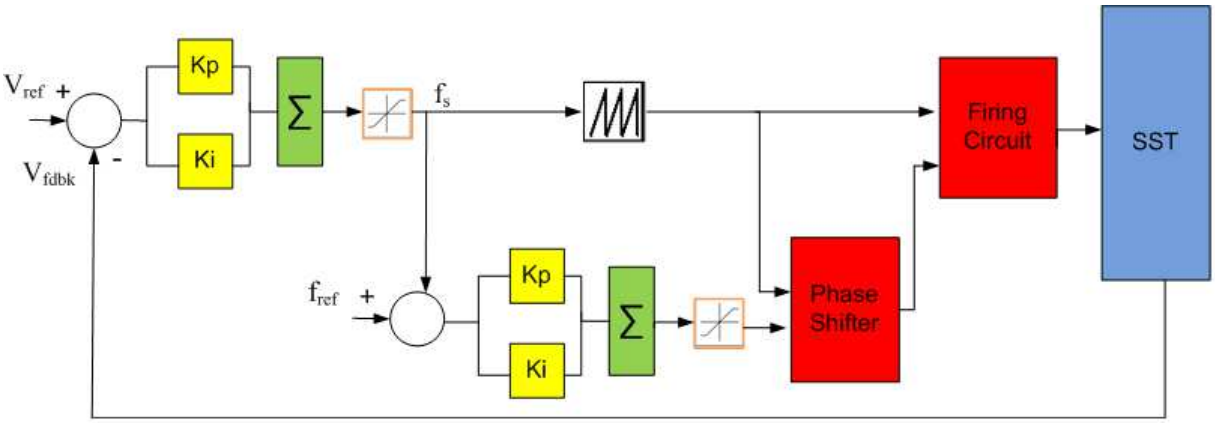


Figure 4-3: SST control block diagram using two parallel PI loops.

Figure 4-4 shows a high level block diagram of the proposed controller. G1 and G2 correspond to gates 1 and 2, respectively. The switching sequence of these two switches is only governed by the switching frequency *fs*. The leading leg in the H-bridge is the leg that consists of switches 1 and 2. The switching sequence in the lagging leg, however, is governed by both the switching frequency *fs* and the phase shift angle α.

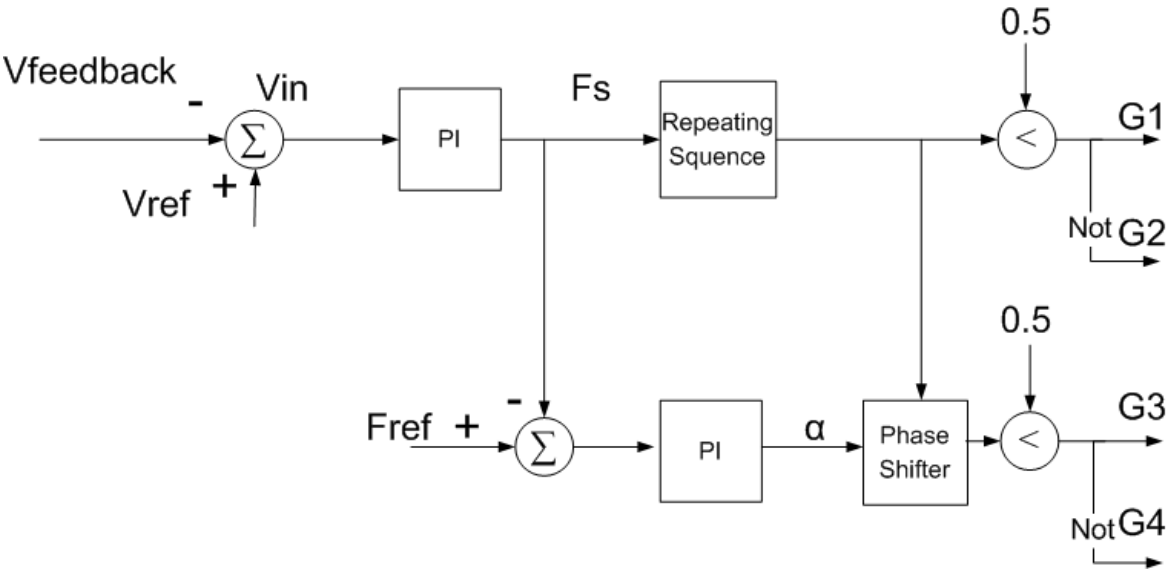


Figure 4-4: High level block diagram of the proposed controller.

There's a sampling delay on the switching frequency *fs* being fed to the repeating sequence block diagram. The delay guarantees updating the switching frequency not faster than a pre-determined time delay $T_u$. The purpose of the delay is to obtain smooth transition from the input to the output and not have the switching frequency change at a very high rate, which distorts the operation of the switches. Within that interval of the delay $T_u$, the switching frequency appears constant to the rest of the circuit.

Therefore, the phase shifter, which has a faster response, updates the value α and changes the level of current being sent to the output load. The minimum phase shift corresponds to "α=15%" whereas the maximum phase shift corresponds to "α=95.75%", which is cancelling 95.75% of the duty cycle.

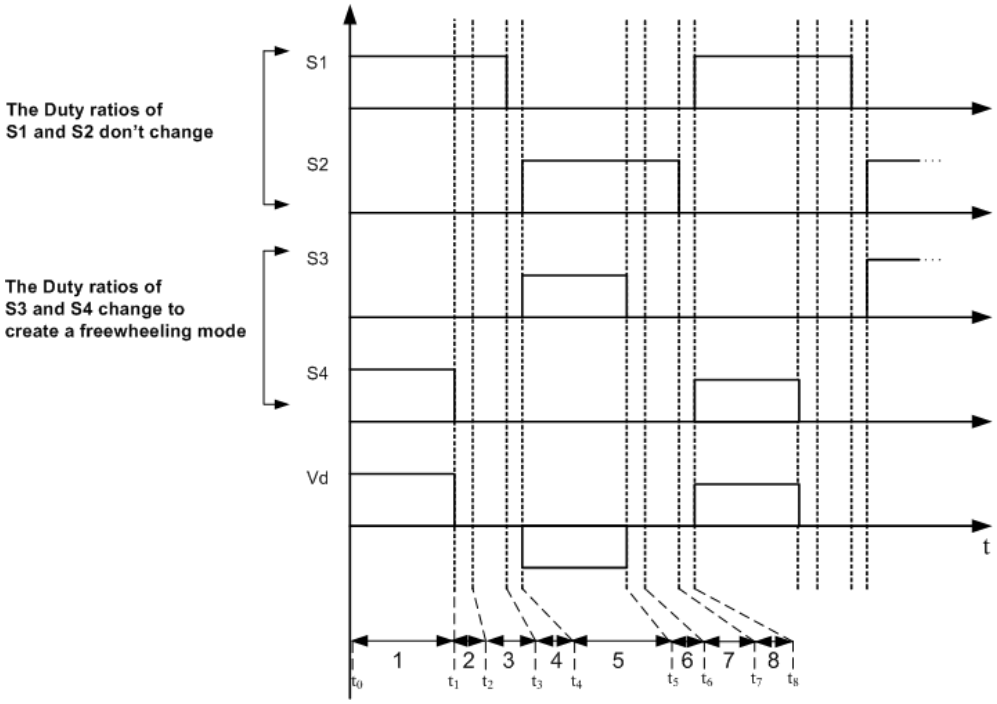


Figure 4-5: Gate signals and the corresponding inverter voltage.

### 4.2 Control Implementation:

The simulation of the circuit and the controller was performed using Simulink and PLECS. Simulink was used to build the controller and generate the gate signals G1 through G4. PLECS was used to simulate the SST and investigate the switching transients of the four switching devices.

Table 4 summarizes the parameters used in the simulation. $PI_1$ and $PI_2$ correspond to the two PI controllers in the PSM and PFM control loops, respectively.

| Parameter | Rating |
|---|---|
| Lr | 10 µH |
| Lm | 200-300 µH |
| Cr | 4 µF |
| Cout | 1000 uF |
| Rout | 100 ohms- at high load |
| | 200 ohms- at low load |
| $PI_1$ | Kp=1<br>Ki=0.0001 |
| $PI_2$ | Kp=0.4<br>Ki=20 |
| Vin | 700 V |

Table 4. Parameters of the system.

The selection of these parameters guarantees that a switching frequency *fs* of 30 KHz is above the resonant frequency of the system. In addition, the selection of the magnetizing inductance Lm is limited by equation (17).

Figure 4-6 shows the connection between the controller and PLECS circuit built using its blockset from Simulink. PLECS appears to have better dynamics and/or options when it comes to running heavy power electronic simulations. In addition, PLECS is very useful in investigating the switching transients of the IGBTS i.e. the turn ON/OFF transitions. It's also excellent for conducting thermal analysis to determine losses and efficiency (more on that in chapter 4).

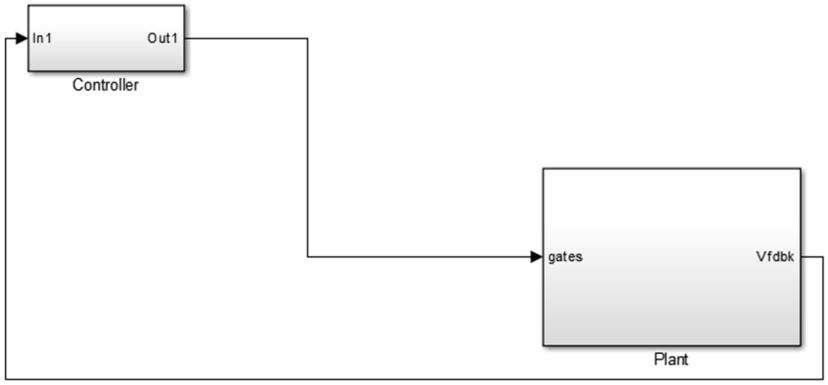


Figure 4-6: Simulation blocks using Simulink and blockset PLECS in Matlab/Simulink.

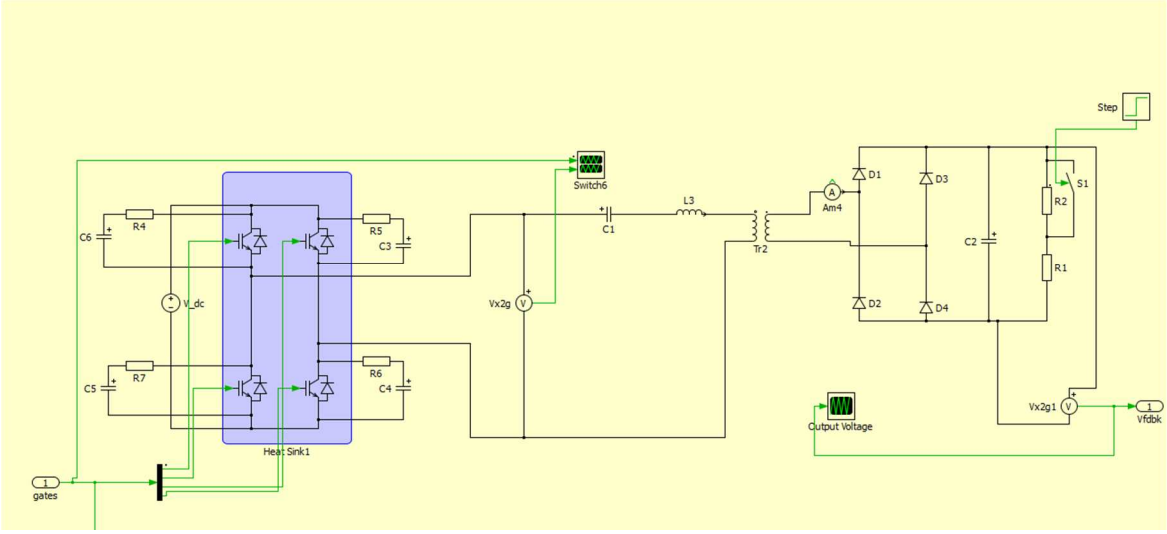


Figure 4-7: SST simulation in PLECS (heat sink in blue).

The disturbance response of the controller was tested by changing the load on the output from high to low as described in table1. The output voltage is regulated at 1000v. Looking at figure 3-4, operating above fr2 implies that increasing *fs* decreases the gain of the converter. Therefore, the PFM controller reacts to the event of a sudden decrease of the load by increasing the switching frequency *fs* to reach a point on the gain curve that matches the required output voltage. As the switching frequency increases, the PSM controller increases the phase shift α. This results in a decrease in the switching frequency, and by selecting "$F_{ref}$", it is possible to operate at different points of figure 4-2. Figure 4-8 shows the load voltage at the described event of load change. A very small disturbance of 0.22% occurs. The change in fs is shown in figure 4-9 where the switching frequency is driven to the desired reference, which is 30 kHz in this case. The output voltage of the H-bridge at high and low load is shown in figure 4-10. The angle of phase

shift “α” can be noticed by looking at the gate signals of switches ‘3’ and ‘4’. Comparing figure 10(a) to figure 10(b), phase shift is larger in the case of smaller load. The switching frequency *fs* is driven back to its reference value after the disturbance is cleared by adjusting the phase shift.

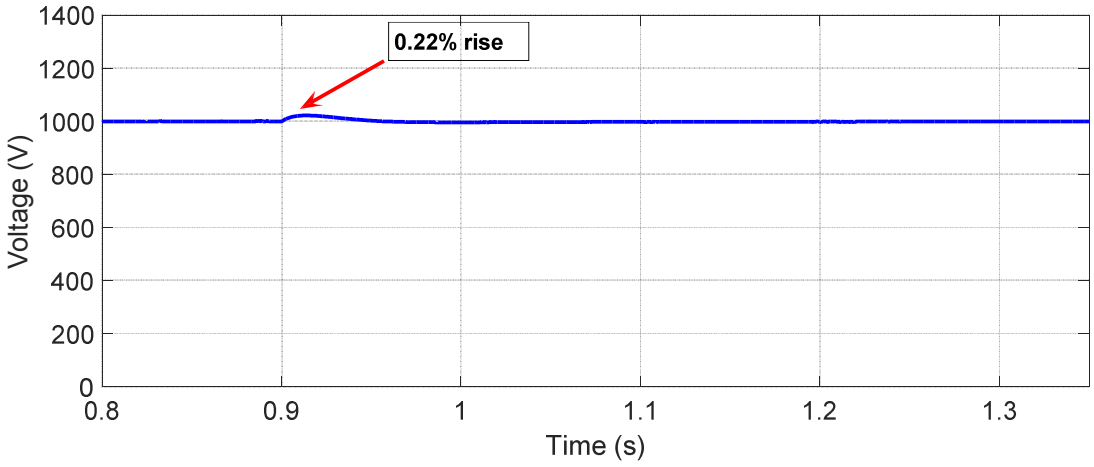


Figure 4-8: Load Voltage Response.

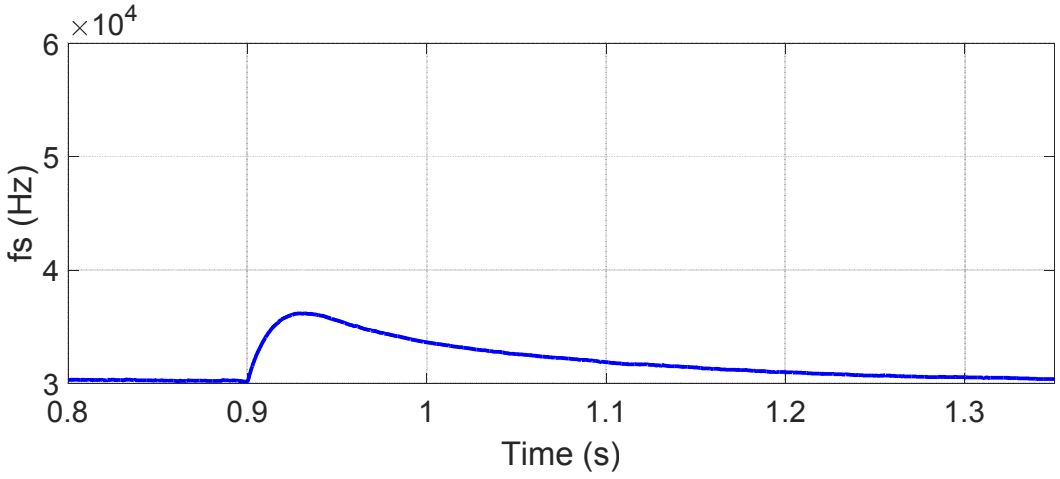


Figure 4-9: Switching Frequency Response.

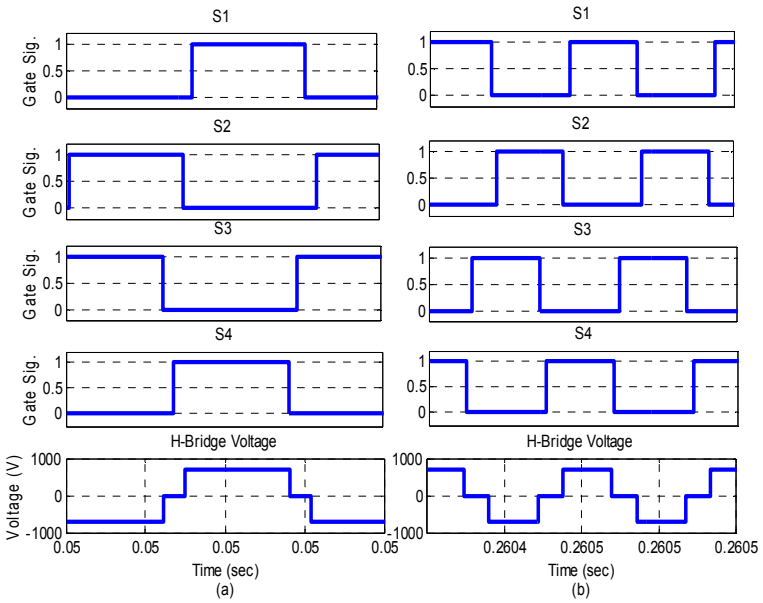


Figure 4-10: H-bridge output voltage: a) High load b) low load.

Figure 4-11 shows the switching transient of all four switches. One of the main drives behind this research is to achieve ZVS and ZCS. As can be seen in the figure, ZVS was achieved for turn ON for all switches, while ZCS turn off was achieved for the switches in the lagging leg ($S_1$ and $S_2$).

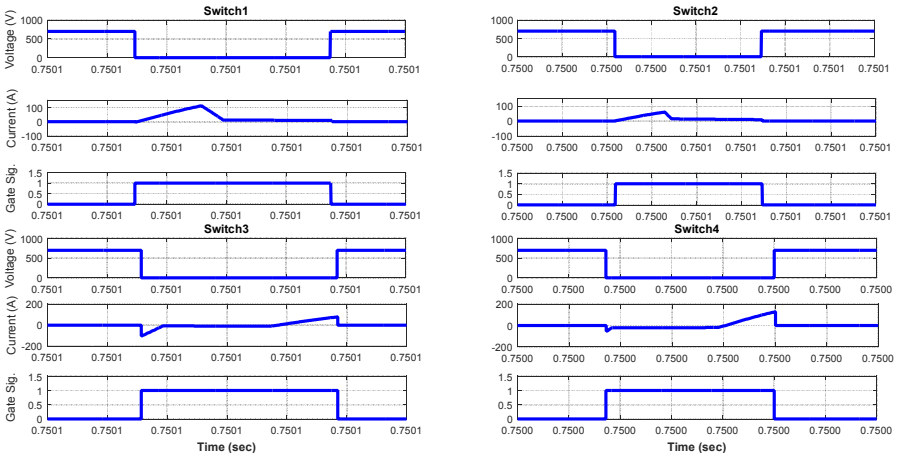


Figure 4-11: Turn ON/OFF of switches 1 through 4.

Looking at the resonant current in the series inductor, the freewheeling duration is larger in the case of low load, reason being more phase shift has been enforced by the controller (figures 4-12 and 4-13). In addition, switches 1 and 2 turn off at almost zero current. The amount of current going through the switches at turn off is dictated by the magnetizing inductance Lm. Increasing Lm would result in switching at lower currents and reducing losses. One observed disadvantage, however, is the resulting wider range in switching frequency.

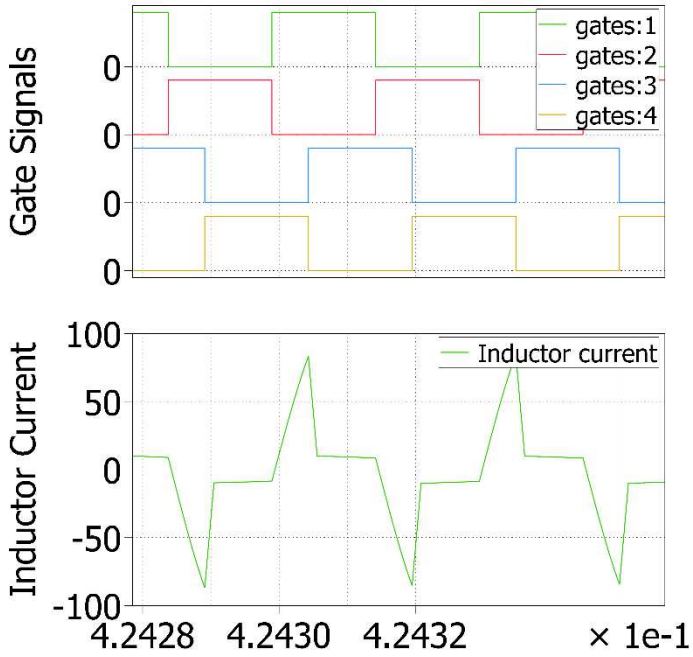


Figure 4-12: Gate signals and inductor current at high load.

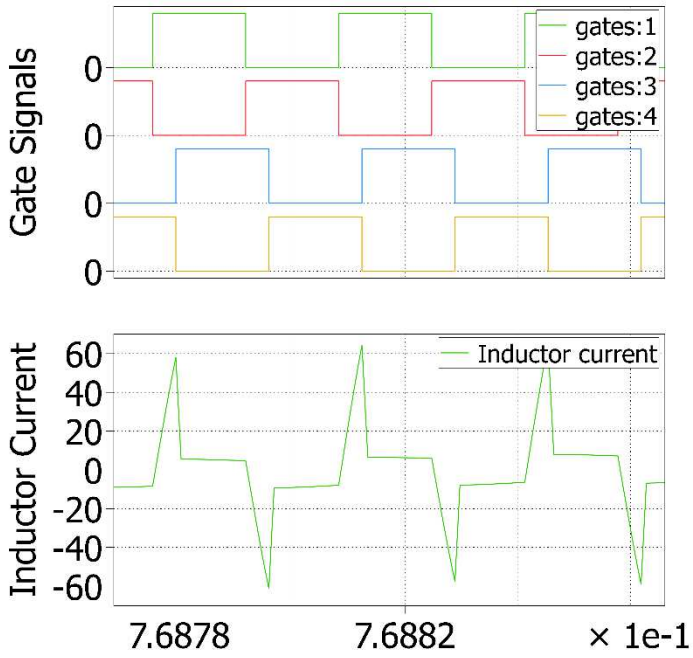


Figure 4-13: Gate signals and inductor current at low load.

### 4.3 Bidirectional Power Flow

In micro grid applications, it is a requirement that power can be transferred from or into a source. For example, a battery can be charged for some duration and discharged for another. If the diode rectifier bridge is replaced by a controlled full h-bridge, bidirectional power flow can be achieved. In the proposed SST topology, the same concept of PSM can be applied to create a phase-shift between the primary H-bridge voltage $V_p$, and the secondary H-bridge voltage $V_s$. If $V_p$ leads $V_s$, power flows from the primary side to the secondary side, whereas if $V_s$ leads $V_p$ power flows from the secondary to the primary side. Figure 4-14 shows the respective waveforms.

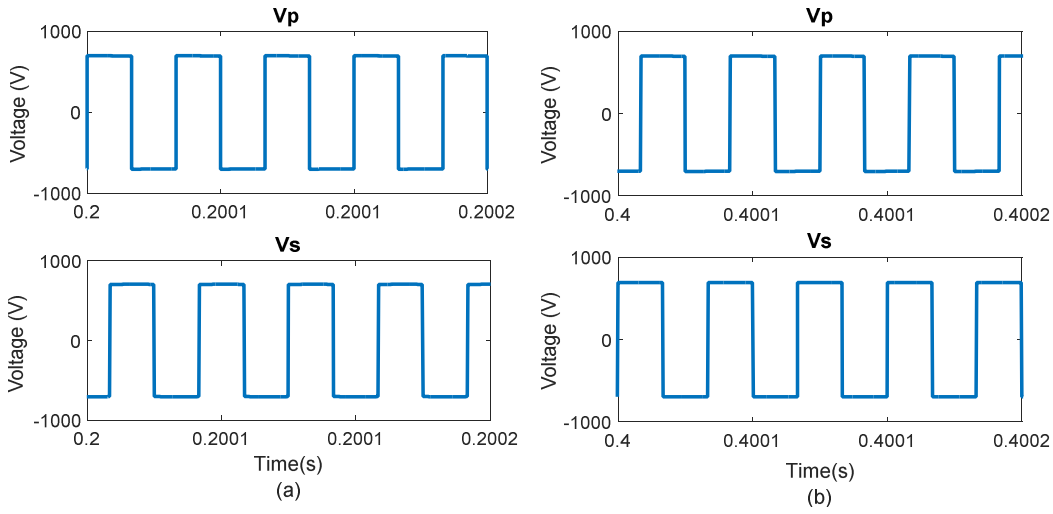


Figure 4-14: Primary ($V_p$) and secondary ($V_s$) voltages: a) $V_p$ leads $V_s$ b) $V_p$ lags $V_s$.

The transfer from the state in figure 4-14(a) to the state in figure 4-14(b) is done during runtime at time t=0.35s. The resulting waveform of the secondary current is shown in figure 4-15. The change in current flow from positive to negative indicates the change in the power flow.

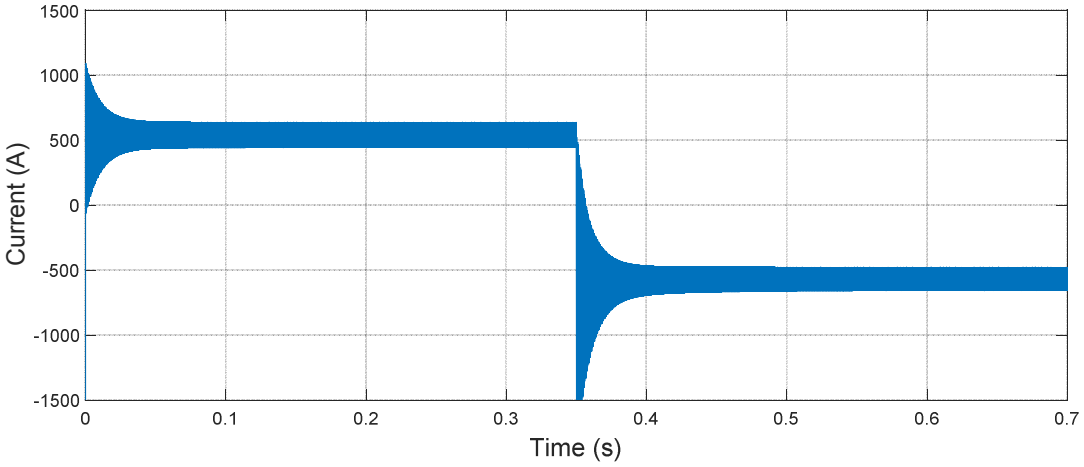


Figure 4-15: Secondary output current.

By changing the phase shift between the primary and secondary sides, power flow can be controlled. The amount of power being controlled by the phase angle difference is given by [14]:

$$p = \frac{nV_{dc1}V_{dc2}D(1-D)}{2f_sL} \quad (25)$$

Where the equation parameters are as follows:

n: turns ratio of the transformer

$V_{dc1}$: primary side dc voltage

$V_{dc2}$: primary side dc voltage

D: (phase shift)/π

$f_s$: switching frequency

L: series inductance in the converter

Looking at equation (25), the output current is then [14]:

$$I_o = \frac{nV_{dc1}D(1-D)}{2f_sL} \tag{26}$$

### 4.4 Multiport Application

One more requirement that is often brought up in micro grid applications is multiport converters. Although this is not the main focus of this thesis, but a simulation was performed to act as a building block for future work. The necessity of multiport converters rises from the fact that multiple sources, loads and a grid connection should all be taken into account when designing a micro grid. Section 4.3 discussed the operation of two sources using a bidirectional SST. In this section, the secondary source is replaced by a resistive load. However, both H-bridges on the primary and secondary use active switches (IGBT's) and are actively controlled. Again, phase shifting the primary voltage $V_p$ and the secondary voltage $V_s$ controls the current being sent from the primary stage to the secondary stage. By adjusting this phase shift, voltage is regulated. This is shown in figure 4-16 where voltage is regulated at 400v.

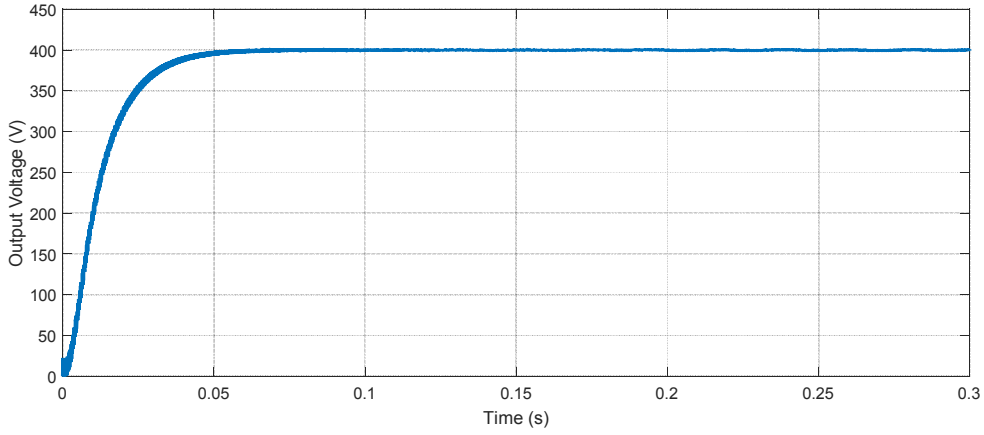


Figure 4-16: Voltage regulation of the DAB.

# CHAPTER V

## 5. THERMAL ANALYSIS:

Switching at high frequency may increase the dissipated heat. Therefore, conducting a thermal analysis is crucial in designing such power converters. Many switching devices with different characteristics are available in the market, and depending on the application, the most suitable devices should be selected. With a good understanding of the thermal behavior of the converter, a heat sink and a cooling method can be selected. This chapter discusses the sources of losses in the converter and its simulation.

### 5.1 Loss Calculation:

For switching devices, there are typically two sources of losses, switching and conduction losses. Switching losses are the sum of turn on and turn off losses. In this work, operation is in super resonance, so turn on losses are null. Turn off losses are the main source of switching losses. Conduction losses are seen across all four switches. Figures 5-1 and 5-2 show the datasheet specifications for losses for the selected IGBT.

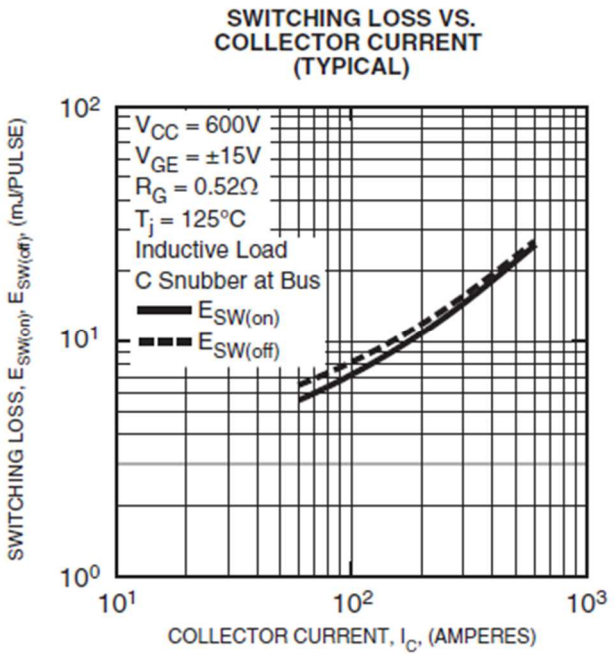


Figure 5-1: Switching losses as specified in the IGBT's datasheet.

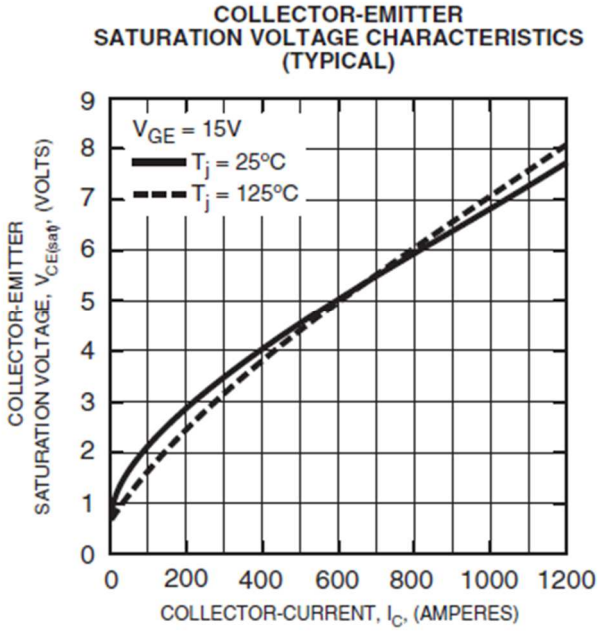


Figure 5-2: Saturation characteristics as specified in the data sheet.

## 5.2 PLECS Simulation:

A thermal analysis was conducted using a user defined thermal library in PLECS. Turn on and turn off were estimated using the manufacturer's datasheet by using Eon and Eoff, the on-state and off-state energy dissipation in the switches respectively. Figures 5-3 and 5-4 show the curves entered to PLECS to calculate the turn on and turn off losses, respectively. Table 5 summarizes the resulting calculated switching losses for the four switches. Figure 5-5 shows the curves entered to PLECS to calculate the conduction losses of the switches. Table 6 summarizes the resulting conduction losses.

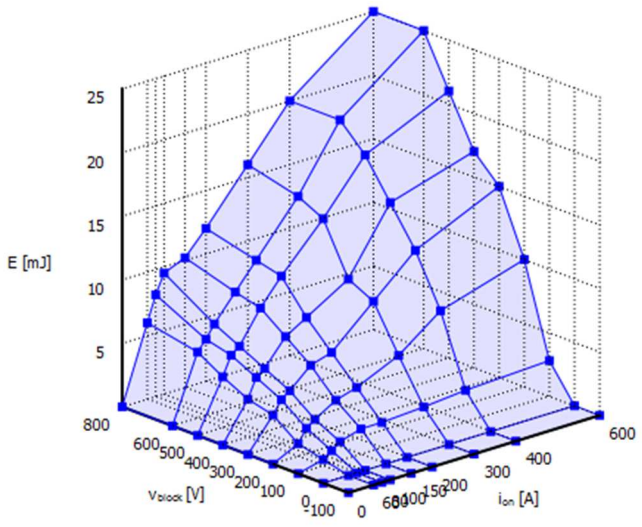


Figure 5-3: Turn on losses curve.

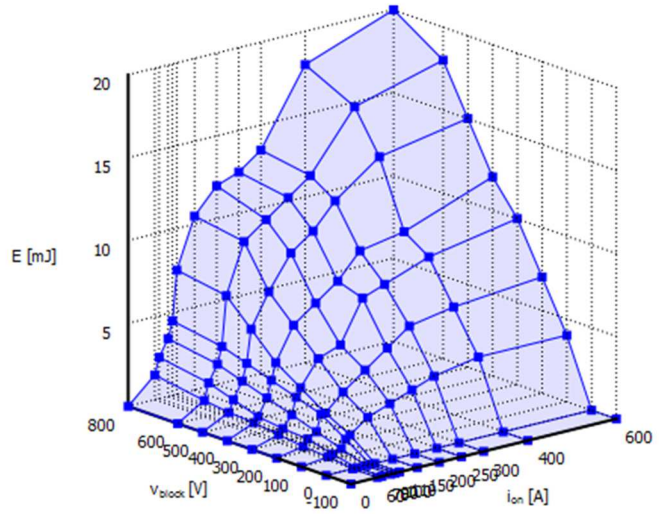


Figure 5-4: Turn off losses curve.

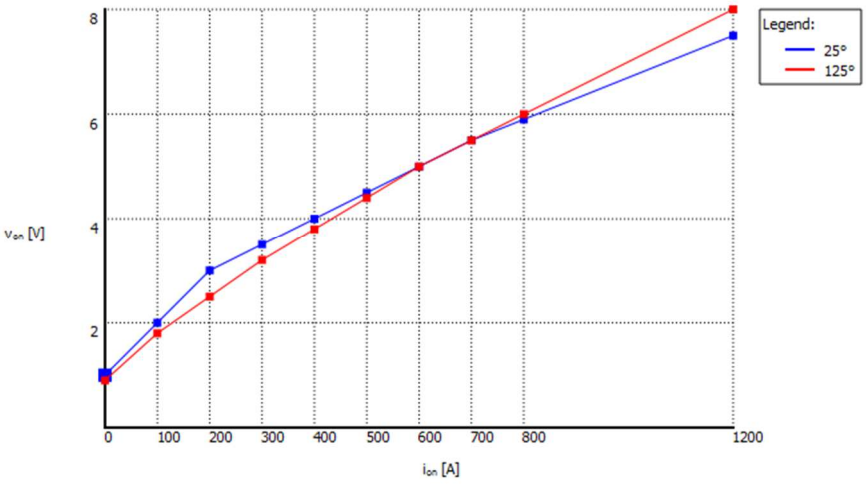


Figure 5-5: Conduction losses curve.

Looking at tables 5 and 6, switching losses are significantly reduced in switches 1 and 2. These two switches turn off at ZCS. Switches 3 and 4 switches turn off at a finite current, giving rise to higher switching losses. Conduction losses, however, are larger in switches 1 and 2 due to the larger duty cycle.

| | |
|---|---|
| Switch1 | High load: 10.85 W |
| | Low load: 7.88 W |
| Switch 2 | High load: 10.48 W |
| | Low load: 7.81 W |
| Switch 3 | High load: 108.2 W |
| | Low load: 50.1 W |
| Switch 4 | High load: 106.7 W |
| | Low load: 50.04 W |

Table 5: Per-cycle switching losses.

| | |
|---|---|
| Switch 1 | High load: 15.63 W |
| | Low load:  7.89 W |
| Switch 2 | High load:  15.42 W |
| | Low load: 7.95 W |
| Switch 3 | High load: 9.4 W |
| | Low load: 4.04 W |
| Switch 4 | High load: 9.56 W |
| | Low load: 4.03 W |

Table 6: Per-cycle conduction losses.

# CHAPTER VI

## 6. EXPERIMENTAL TESTING

The series resonant solid state transformer introduced in this study has been designed and assembled to verify the results through lab tests. The prototype is rated at 150 KVA.

### 6.1 Setup

The prototype is composed of an FPGA control board, gate driver board, isolation transformer, 3-phase full bridge rectifier, and full-bridge configuration and output full bridge diodes. To plot the voltage and current, a Tektronic TDS5000 digital oscilloscope along with a high voltage prop were used. Comparing figures 6-1 and 6-2, there's a huge advantage in reduction of size when using SST's that incorporate high frequency planar transformers. The reduction in size is substantial.

Figure 6-1: Solid State Transformer Prototype.

Figure 6-2: Conventional Transformer of comparable power rating.

The resulting h-bridge output voltage, resonant inductor current, and output regulated DC voltage are shown in the following section.

## 6.2 Results

Figure 6-2 shows the primary results of the test. Soft start was used to ramp up the output voltage from 0 to the set reference. The converter was run to give 1000 VDC at the output. The yellow (upper) curve shows the output DC which the converter regulates properly. The purple curve is the gate signal and the green (lower) curve is the primary ac current of the HF transformer. Figures 6-3 and 6-4 show the startup waveforms of the converter where pulses of current were applied for very short periods of time. In figure 6-5 the load power is low and consumes only 15kW. The SST can handle up to 150kW. In the next test the converter was almost close to its nominal power rating, figure 6-6 shows the resulting waveforms. This is evident by looking at the terminal voltage of the inverter (purple) square wave signal. Phase shifting in this case is minimal and the controller takes

advantage of most of the duty cycle. Therefore, the converter meets the power demand by increasing the duty cycle and decreasing the switching frequency, while maintaining soft switching. Comparing the results of low and high load test it can be seen that the more load power, the bigger duty ratio, and the current waveform is more sinusoidal.

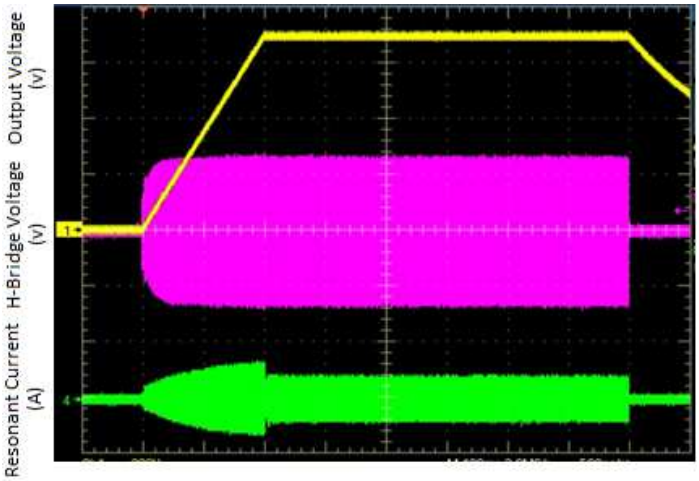


Figure 6-3: Output DC, Gate signal and HF Primary current of the SST.

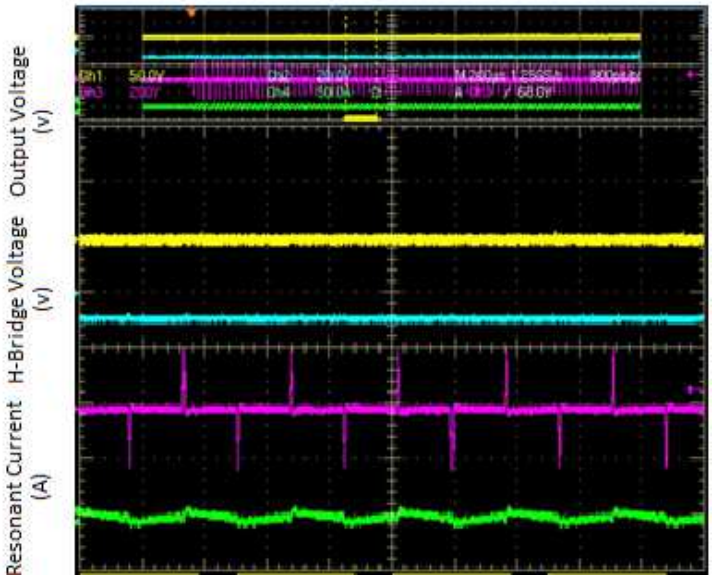


Figure 6-4: Converter Test Results during startup.

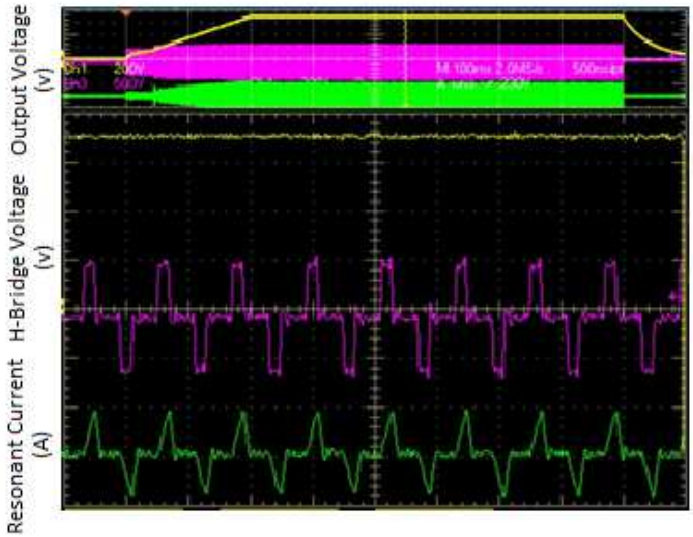


Figure 6-5: Converter Test Results for low power load of 15kW.

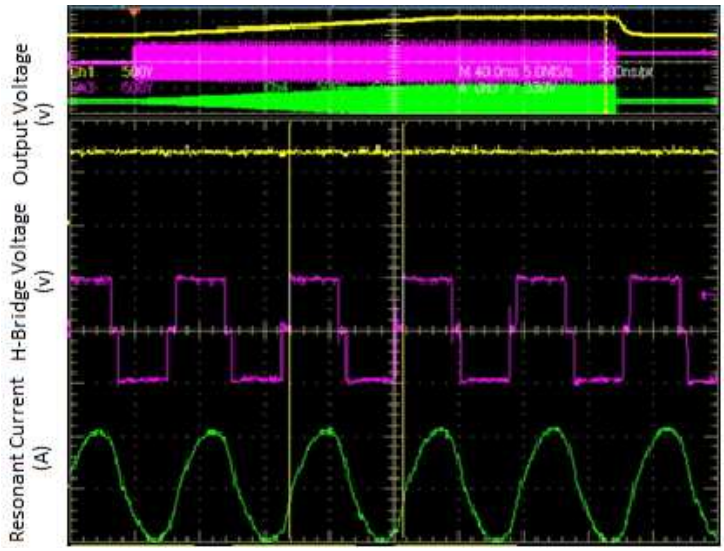


Figure 6-6: Converter Test Results for high power load of 140kW.

# CHAPTER VII

## 7. SUMMARY AND CONCLUSION

A new control structure has been introduced for an LLC resonant SST. The discussed topology has several advantages compared to conventional topologies that rely only on transformers or only on power electronics circuitries. It provides load regulation, power flow control, and galvanic isolation. By adding a resonant tank and designing its parameters, soft-commutation has been achieved. The proposed controller adjusts the output voltage of the system by varying the switching frequency *fs* and the phase shift $\alpha$ between the two legs of the H-bridge. Simulation results using Simulink and PLECS were discussed in this work. Simulink was used to implement the controller where PLECS was used to simulate the circuit topology. Experimental testing on a 150 KVA prototype SST was conducted. Starting of the circuit until it reaches steady state is shown, as well as low power load and high power load test results. These experimental results comply with the simulation results.

For future work, there are numerous areas that can be explored. The use of SiC devices in SST topologies can help in reducing size and minimizing cost. At higher switching frequencies, losses can be reduced by using SiC devices. In addition, extending the concept of resonance to multiport, multilevel, and DAB topologies is a recommended area of research. Multiport topologies are essential in microgird applications, and their analysis and design is harder than two-port topologies. Finally, one more topic to be researched is three phase SST's and applying resonance to achieve soft commutation in such topologies.

# REFERENCES


[1] Ahmedabad, Gujarat," Solid State Transformer (SST) "Review of Recent Developments", in *Advance in Electronic and Electric Engineering, 2014. Research India Publications,* Vol. 5, No. 1, pp. 40-50, (2014).

[2] J. W. Kolar, G. Ortiz, "Solid State Transformer Concepts in Traction and Smart Grid Applications", *Tutorial at the 15th International Power Electronics and Motion Control Conference (ECCE Europe 2012)*, Novi Sad, Serbia, September 4-6, 2012.

[3] S. Xu, A. Q. Huang, R. Burgos, "Review of Solid-State Transformer Technologies and Their Application in Power Distribution Systems," *IEEE Journal of Emerging and Selected Topics in Power Electronics*, vol. 1, no. 3, pp. 186-198, 2013.

[4] Jung, J-.H.; Kim, H-.S.; Ryu, M-.H.; Baek, J-.W., "Design Methodology of Bidirectional CLLC Resonant Converter for High-Frequency Isolation of DC Distribution Systems," in *Power Electronics, IEEE Transactions on* , vol.28, no.4, pp.1741-1755, April 2013.

[5] M. S. Agamy and P. K. Jain, "A Variable Frequency Phase-Shift Modulated Three-Level Resonant Single-Stage Power Factor Correction Converter," in *IEEE Transactions on Power Electronics*, vol. 23, no. 5, pp. 2290-2300, Sept. 2008.

[6] K. Tan, R. Yu, S. Guo and A. Q. Huang, "Optimal design methodology of bidirectional LLC resonant DC/DC converter for solid state transformer application," *Industrial Electronics Society, IECON 2014 - 40th Annual Conference of the IEEE*, Dallas, TX, 2014, pp. 1657-1664.

[7] Q. Huang, K. Shi, X. Jia, C. Hu and D. Xu, "A bi-directional resonant DC/DC converter with frequency tracking control," *Energy Conversion Congress and Exposition (ECCE), 2014 IEEE*, Pittsburgh, PA, 2014, pp. 4748-4754.

[8] Jee-hoon Jung and Joong-gi Kwon, "Theoretical analysis and optimal design of LLC resonant converter," *Power Electronics and Applications, 2007 European Conference on*, Aalborg, 2007, pp. 1-10.

[9]K. Murata and F. Kurokawa, "An Interleaved PFM LLC Resonant Converter With Phase-Shift Compensation," in *IEEE Transactions on Power Electronics*, vol. 31, no. 3, pp. 2264-2272, March 2016.

[10] P. Wang, C. Liu, L. Guo, "Modeling and Simulation of Full-Bridge Series Resonant Converter Based on Generalized State Space Averaging", *Applied Mechanics and Materials*, Vols. 347-350, pp. 1828-1832, 2013

[11] S. Chudjuarjeen, Anawach Sangswang and C. Koompai, "An improved LLC resonant inverter for induction heating with asymmetrical control," *2009 IEEE International Symposium on Industrial Electronics*, Seoul, 2009, pp. 1612-1617. [12] J. Jittakort, S. Yachiangkam, A. Sangswang, S. Naetiladdanon, C. Koompai and S. Chudjuarjeen, "A variable-frequency asymmetrical voltage-cancellation control of series resonant inverters in domestic induction cooking," *Power Electronics and ECCE Asia (ICPE & ECCE), 2011 IEEE 8th International Conference on*, Jeju, 2011, pp. 2320-2327.

[13] J. Hiltunen, V. Väisänen, R. Juntunen and P. Silventoinen, "Variable-Frequency Phase Shift Modulation of a Dual Active Bridge Converter," in *IEEE Transactions on Power Electronics*, vol. 30, no. 12, pp. 7138-7148, Dec. 2015.

[14] J. Shi, W. Gou, H. Yuan, T. Zhao and A. Q. Huang, "Research on voltage and power balance control for cascaded modular solid-state transformer," in *IEEE Transactions on Power Electronics*, vol. 26, no. 4, pp. 1154-1166, April 2011.

[15] S.D. Zambrano, "A DC-DC Multiport Converter Based Solid State Transformer Integrating Distributed Generation and Storage," Ph.D. dissertation, Dept. Elect. Eng., Arizona State Univ., Phoenix, Arizona, 2011.

[16] D. Shanmugam and K. Indiradevi, "Implementation of multiport dc-dc converter-based Solid State Transformer in smart grid system," *Computer Communication and Informatics (ICCCI), 2014 International Conference on*, Coimbatore, 2014, pp. 1-6.

[17] H.M. Chou, “Multi-port DC-DC Power Converter for Renewable Energy Application,” M.S. thesis, Dept. Elect. Eng., Texas A&M University, College Station, Texas, 2009.
[18] D. Han and B. Sarlioglu, "Study of the switching performance and EMI signature of SiC MOSFETs under the influence of parasitic inductance in an automotive DC-DC converter," *Transportation Electrification Conference and Expo (ITEC), 2015 IEEE*, Dearborn, MI, 2015, pp. 1-8.
[19] N. Mohan, “Resonant Converters,” in *Power Electronics: Converters, Applications and Design*, Minneapolis MN: John Wiley & Sons, INC., 1989, Ch. 9.
[20] W. McMurray, "The Thyristor Electronic Transformer: a Power Converter Using a High-Frequency Link," in *IEEE Transactions on Industry and General Applications*, vol. IGA-7, no. 4, pp. 451-457, July 1971.
[21] X. She, R. Burgos, G. Wang, F. Wang and A. Q. Huang, "Review of solid state transformer in the distribution system: From components to field application," *2012 IEEE Energy Conversion Congress and Exposition (ECCE)*, Raleigh, NC, 2012, pp. 4077-4084.
[22] X. She and A. Huang, "Solid state transformer in the future smart electrical system," *2013 IEEE Power & Energy Society General Meeting*, Vancouver, BC, 2013, pp. 1-5.
[23] M. Barnes *et al*., "Real-World MicroGrids-An Overview," *2007 IEEE International Conference on System of Systems Engineering*, San Antonio, TX, 2007, pp. 1-8.
[24] R. Erikson and D. Maksimovic’, “Resonant Conversion,” in *Fundaments of Power Electronics*, Boulder CO: Springer Science and Business Media Inc., 1997, Ch. 19.
[25] E. Mekonam, “Medical Grade High Frequency Power Distribution Units”, M.S. thesis, Dept. Elect. Eng., Univ. Wisconsin. Milwaukee, USA, 2012.
[26] D. Boroyevich, I. Cvetković, D. Dong, R. Burgos, F. Wang and F. Lee, "Future electronic power distribution systems a contemplative view," *Optimization of Electrical and Electronic Equipment (OPTIM), 2010 12th International Conference on*, Basov, 2010, pp. 1369-1380.
[27] V. Dutta, “Modeling, Control and Test of the Dual Active Bridge Converter for applications in modular, high power, Solid State Transformers,” Ph.D. dissertation, Dept. Elect. Eng., University College Dublin, Dublin, Ireland, 2015.
[28] H. Qin, “Dual Active Bridge Converters in Solid State Transformers,” Ph.D. dissertation, Dept., Elect. Eng., Missouri University of Science and Technology, Rolla, Missouri, 2012.
[29] X. She, “Control and Design of a High voltage Solid State Transformer and its Integration with Renewable Energy Resources and Microgrid System,” Ph.D. dissertation, Dept., Elect., Eng., North Carolina State University, Raleigh, North Carolina, 2013.
[30] X. She, A. Q. Huang, S. Lukic, and M. E. Baran, “On Integration of Solid-State Transformer With Zonal DC Microgrid,” *IEEE Trans. Smart Grid*, vol. 3, no. 2, pp. 975–985, 2012.
[31] X. She, S. Lukic, A. Q. Huang, S. Bhattacharya, and M. Baran, “Performance evaluation of solid state transformer based microgrid in FREEDM systems,” *Proc. IEEE APEC*, pp. 182–188, 2011.
[32] X. She, S. Lukic, and Q. H. Alex, “DC zonal micro-grid architecture and control,” in *Proc. IEEE IECON*, 2010, pp. 2988–2993.
[33] H. Kakigano, Y. Miura, and T. Ise, “DC micro-grid for Super High Quality Distribution-System configuration and control of Distributed Generations and Energy Storage Devices,” in *Proc. IEEE PESC*, 2006, pp. 1–7.

# A. APPENDICES

## A.1 Undamped Series-Resonant Circuit

Figure A-1 shows an undamped series-resonant circuit where the input voltage is $V_d$ at time$t_o$. The initial conditions are $I_{LO}$ and $V_{CO}$. With the inductor current $i_L$ and the capacitor voltage $v_c$ as the state variables, the circuit equations are [19]:

$$L_r \frac{di_L}{dt} + v_c = V_d \quad \text{(A-1)}$$

and

$$C_r \frac{dv_c}{dt} = i_L \quad \text{(A-2)}$$

For $t \geq t_o$, the solution is as follows:

$$i_L(t) = I_{Lo} \cos \omega_o(t - t_o) + \frac{V_d - V_{co}}{Z_o} sin\omega_o(t - t_o) \quad \text{(A-3)}$$

and

$$V_c(t) = V_d - (V_d - V_{co})cos\omega_o(t - t_o) + Z_o I_{Lo} sin\omega_o(t - t_o) \quad \text{(A-4)}$$

where the angular resonance frequency = $\omega_o = 2\pi f_o = \frac{1}{\sqrt{L_r C_r}}$ (A-5)

and Characteristic impedance = $z_o = \sqrt{\frac{L_r}{C_r}}$ (A-6)

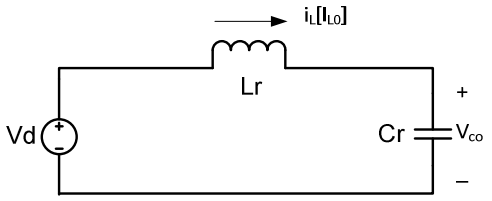


Figure A-A-1: Undamped series-resonant circuit [19].

## A.2 Series Resonant Circuit with a Capacitor Parallel Load

Figure A-2 shows series resonant circuit, where the capacitor is loaded in parallel with $I_o$. In this circuit, $V_d$ and, $I_o$ are dc quantities. The initial conditions are $I_{LO}$ and$V_{CO}$ at time $t_o$ [19]. Therefore:

$$v_c = V_d - L_r \frac{di_L}{dt} \tag{A-7}$$

and $$i_L - i_c = I_o \tag{A-8}$$

By differentiating Eq. A-7

$$i_c = C_r \frac{dv_c}{d_t} = -L_r C_r \frac{d^2 i_L}{dt^2} \tag{A-9}$$

Substituting $i_c$ from Eq. A-9 into Eq. A-8 yields

$$\frac{d^2 i_L}{dt^2} + \omega_o^2 i_L = \omega_o^2 i_o \tag{A-10}$$

Where angular resonance frequency $\omega_o$is still the same as Eq. (A-5), solution for $t \geq t_o$ is as follow:

$$i_L(t) = I_o + (I_{LO} - I_o) cos\omega_o(t - t_o) + \frac{V_d - V_{co}}{Z_o} sin\omega_o(t - t_o) \tag{A-11}$$

And

$$v_c(t) = V_d - (V_d - V_{co}) cos\omega_o(t - t_o) + Z_o(I_{LO} - I_o) sin\omega_o(t - t_o) \tag{A-12}$$

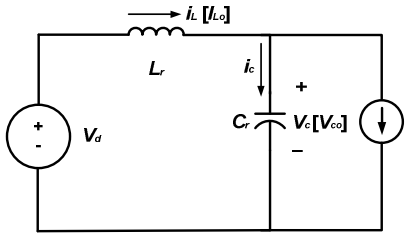


Figure A-2: Series-resonant circuit with capacitor-parallel load [19].